Biomass and Bioenergy 203 (2025) 108273

Contents lists available at ScienceDirect

Biomass and Bioenergy

journal homepage: www.elsevier.com/locate/biombioe

Valorization of pure and biodiesel-derived refined crude glycerol to renewable acetol over copper-based catalyst: Effect of operating conditions and catalyst stability

Alejandro Lete, Lucía García *, Joaquín Ruiz, Jesús Arauzo

ARTICLE INFO

Keywords:
Glycerol
Acetol
Refined crude glycerol
Copper
Dehydration
Deactivation

ABSTRACT

Acetol is a key intermediate in the aldol condensation of biomass-derived furans, enabling the production of carbon chains within the aviation fuel range. This work proposes glycerol, a biomass-derived by-product from biodiesel production, as a renewable feedstock for acetol production. The catalytic performance of a CuAl catalyst was evaluated in the gas phase dehydration of glycerol, focusing on the influence of temperature (200–300 °C), catalyst weight to glycerol mass flow ratio (10–50 $g_{Catalyst}$ min $g^{-1}_{Glycerol}$), and carrier gas to liquid ratio (200–600 m^3_{Gas}STP m^{-3}_{Liquid}). Both pure and biodiesel-derived refined crude glycerol were used as feedstock. Long-term stability experiments assessed the evolution of catalytic activity and physicochemical properties over time. A great activity was obtained under conditions of 250 °C, 30 $g_{Catalyst}$ min $g^{-1}_{Glycerol}$, and 400 m^3_{Gas}STP m^{-3}_{Liquid} with pure glycerol after a time-on-stream (TOS) of 2 h (95.1 % glycerol conversion and 564 mg_{Acetol} $g^{-1}_{Glycerol}$). Stability studies provided good catalytic results after a TOS of 52 h using pure glycerol (72 % glycerol conversion and 266 mg_{Acetol} $g^{-1}_{Glycerol}$) and demonstrated that coke deposition was responsible for catalyst deactivation. The use of refined crude glycerol proved to be highly effective in the first hours of the reaction (98.7 % glycerol conversion and 570 mg_{Acetol} $g^{-1}_{Glycerol}$ for a TOS of 2 h), however, rapid deactivation was observed due to solids deposition. This catalytic route highlights the feasibility of valorization of biomass residues for producing renewable acetol, a promising precursor for sustainable aviation fuel (SAF).

1. Introduction

The negative consequences of climate change and the depletion of oil reserves have accelerated the process of decarbonization in many sectors, stimulating the exploration of novel alternative energy sources to fossil fuels, particularly in aviation. Several aviation organizations, including the International Civil Aviation Organization (ICAO) and the International Air Transport Association (IATA), have set the goal of producing zero net carbon emissions by 2050, which will require the development of sustainable aviation biofuels (SAF) [1,2].

Different methods have been proposed for the production of SAF, these include the Alcohol to Jet Fuels (ATJ), Oil to Jet Fuels (OTJ), or Gas to Jet Fuels (GTJ). However, the high cost of the raw material and the impossibility of producing all the necessary types of hydrocarbons for full use in aviation makes it imperative to explore new pathways for SAF generation [3–6]. In recent years, the Sugar to Jet Fuels (STJ) route has emerged as one of the most promising, allowing the efficient generation of all the necessary types of hydrocarbons in today's aviation fuels [7,8]. The STJ route uses biomass with high sugar content as feedstock for producing furans, generally furfural. These furans then undergo a consecutive two-step process of aldol condensation with ketones (acetol or acetone), followed by hydrogenation, yielding carbon chains suitable for utilization as aviation biofuel [9,10]. However, ketones used in the aldol condensation step are usually derived from fossil resources, so it is necessary to develop new pathways to produce them sustainably and efficiently.

The use of glycerol as a bio-based feedstock has been proposed as a solution for the generation of renewable acetol due to its high availability and reactivity [11–13]. In addition to its role as an intermediate in SAF production, acetol is a versatile compound with various industrial applications. It is used in the chemical industry for synthesizing fine chemicals and polyols, in the food industry as a flavoring agent, and in the textile sector as a safer reducing agent in vat dyeing processes [11, 14]. Glycerol is a commodity chemical that can be used for the

* Corresponding author. Thermochemical Processes Group (GPT) Aragón Institute of Engineering Research (I3A), Universidad de Zaragoza, Mariano Esquillor S/N, 50018, Zaragoza, Spain.
E-mail address: luciag@unizar.es (L. García).

https://doi.org/10.1016/j.biombioe.2025.108273
Received 15 May 2025; Received in revised form 27 July 2025; Accepted 7 August 2025
Available online 18 August 2025

production of a large number of sustainable products, including hydrogen, 1,2-propanediol, acrolein, or acetol [15–23]. Glycerol is the main by-product of biodiesel fabrication through the transesterification of vegetable oils or animal fats. Up to 10 tons of crude glycerol are generated for every 100 tons of biodiesel [24]. The valorization of glycerol would encourage the production of renewable chemicals from biomass in the context of a carbon-neutral circular economy.

The mechanism of glycerol dehydration has been extensively studied [25], and there are two possible reaction routes depending on the catalyst acidity. Catalysts with strong acid sites (Brønsted acids) favor the dehydration of glycerol to acrolein [26,27]. This reaction happens in two consecutive steps. In the first one, the secondary alcohol of glycerol is protonated in a strong acid site to form 3-hydroxypropanal, which is then dehydrated to form acrolein [28]. Various catalysts based on W [29,30], Nb [31], or zeolites [32,33] have been used to generate acrolein from glycerol.

On the other hand, catalysts with weak to moderate acid sites (Lewis's acids) promote the coordination with a primary hydroxyl group, producing the dehydration to 2,3-dihydroxypropene which is then tautomerized leading to the formation of acetol [34,35]. The main catalysts for acetol production from glycerol studied in the literature are based on transition metals (Cu, Ni, Cr, or Co) supported on various oxides, including Al_2O_3, SiO_2, ZrO_2, PO_4, and zeolites [35–41]. This process has been investigated in different catalytic systems. Chiu et al. [42] performed the semi-batch reactive distillation of glycerol at 240 °C with Cr-Cu catalysts, obtaining high conversions (>80 %) and acetol selectivity of over 90 %. Basu et al. [43] reported the selective dehydration of glycerol at 220 °C in a batch reactor with a $Cu_2Cr_2O_5/SiO_2$ catalyst for 3 h, resulting in a conversion of 100 % and acetol selectivity of 69 %. However, these systems are not attractive for industrial scaling and a continuous process using an efficient heterogeneous catalyst would allow for higher production volumes and shorter processing times.

Ni and Cu are the main active metals employed in heterogeneous catalysts for acetol production, due to their abundance, cost-effectiveness, and favorable catalytic activity. Ni tends to cleave C-C bonds, increasing the formation of undesirable by-products and reducing selectivity towards acetol [44,45]. Conversely, Cu is more effective in dehydration and hydrogenation reactions, as it efficiently breaks C-O bonds while minimizing the breakage of C-C bonds [46,47]. This fact was proved by a study conducted by Miranda et al. [48] on bimetallic Ni-Cu/γ-Al_2O_3 catalysts at 400 °C with a W/m (catalyst weight to glycerol mass flow) of 45.5 $g_{Catalyst}$ min $g^{-1}_{Glycerol}$, which concluded that the addition of Ni reduced the selectivity to acetol due to the formation of gaseous products such as CH_4 and less degraded alcohols like acetaldehyde or ethylene glycol. Similarly, in a previous study [49], we compared the catalytic activity of NiAl and CuAl catalysts under similar operating conditions of 227 °C and a W/m of 10 $g_{Catalyst}$ min $g^{-1}_{Glycerol}$, demonstrating that Cu is more selective towards acetol due to the reduced generation of secondary products. In spite of this, the primary limitation of Cu catalysts is their low stability, attributed to coke deposition and particle sintering.

Although significant progress has been made in continuous glycerol dehydration to acetol using Cu-based catalysts, there is limited research on the influence of reaction parameters. Prior research on Cu catalysts examined the effect of calcination temperature and atmosphere, demonstrating that calcination under an inert N_2 atmosphere at 675 °C enhanced the selectivity of glycerol to acetol [50]. Moreover, most previous studies focused on reaction times under 5 h, with minimal deactivation, highlighting the need for longer runs to better understand deactivation.

In light of the above, this study investigates the influence of temperature (200–300 °C), catalyst weight to glycerol mass flow ratio (10–50 $g_{Catalyst}$ min $g^{-1}_{Glycerol}$), and carrier gas to liquid ratio (200–600 m^3_{Gas} STP m^{-3}_{Liquid}) on the production of acetol from glycerol over an efficient CuAl catalyst previously reported [50]. Special attention has been paid to the evaluation of catalyst performance during the reaction, including stability studies lasting up to 52 h to uncover deactivation mechanisms. To achieve this, a CuAl catalyst was synthesized through the coprecipitation method and used in a fixed-bed reactor using commercial pure glycerol and refined crude glycerol obtained from the biodiesel production process, specifically from the transesterification of sunflower oil. This research seeks to demonstrate the feasibility of using refined crude glycerol for selective acetol production. The physicochemical properties of both fresh and spent catalysts were evaluated using various characterization techniques (ICP-OES, N_2 adsorption-desorption, H_2-TPR, NH_3-TPD, XRD, XRF, XPS, FESEM, EDS, TGA, and elemental analysis).

2. Material and methods

2.1. Catalyst synthesis

A catalyst denoted as CuAl was synthesized by the coprecipitation method with 28 mol% Cu expressed as Cu/(Cu + Al). The preparation method consisted of dissolving 50.7 g of copper (II) nitrate trihydrate (Merck, ≥99.5 %, CAS: 10031-43-3) and 202.5 g of aluminum nitrate nonahydrate (Fluka Analytical, ≥98.0 %, CAS: 7784-27-2) in 600 mL of mili-Q water at 40 °C under constant stirring. When nitrates were dissolved, an ammonium hydroxide solution of 30 % (Carlo Erba, CAS: 1336-21-6) was added slowly until a pH of 6 was reached. The final pH was established to precipitate copper hydroxides and to avoid copper resolution by ammonium complexes. The resulting mixture was dried at 105 °C overnight and calcined at 500 °C in a muffle for 3 h in an air atmosphere. The resulting catalyst was sieved to a mesh size of 160–315 μm. This catalyst was also used in a previous study [50].

2.2. Refined crude glycerol preparation

The refined crude glycerol was obtained as a by-product of biodiesel produced in the laboratory. Biodiesel was synthesized by catalytic transesterification of sunflower oil with potassium hydroxide (KOH) (VWR Chemicals, 99.2 %, CAS: 1310-73-2) as a homogeneous catalyst and methanol (Carlo Erba, ≥99.0 %, CAS: 67-56-1) as aliphatic alcohol. For the preparation, a molar ratio of 1/6 of oil/methanol and a catalyst weight of 1 % of the oil mass were used, following the experimental procedure described by García et al. [51]. The liquid product was separated by decantation into two phases: upper biodiesel-rich and lower glycerol-rich, known as crude glycerol. For purification, crude glycerol was neutralized with acetic acid (Sigma-Aldrich, ≥99.0 %, CAS:64-19-7) to a final pH of 6 followed by a vacuum distillation to remove methanol and acetic acid residues [52]. Finally, the mixture was decanted, and the purified refined crude glycerol was obtained. The main properties of crude and refined crude glycerol are shown in Table 1.

Table 1
Properties of crude and refined crude glycerol.

	Crude glycerol	Refined crude glycerol
Chemical composition		
Glycerol (wt%)	67.61 ± 2.19	79.94 ± 2.43
Methanol (wt%)	23.20 ± 2.01	4.55 ± 0.32
Acetic acid (wt%)	0	3.99 ± 0.24
Ashes (wt%)	7.68 ± 0.14	9.06 ± 0.21
Water (wt%)	1.51 ± 0.08	2.46 ± 0.14
Elemental analysis		
C (%)	43.90 ± 0.54	35.14 ± 0.91
H (%)	9.63 ± 0.55	8.06 ± 0.32
O (%)[a]	38.79 ± 0.78	47.74 ± 0.99
Physical characteristics		
pH	13.37 ± 0.05	5.83 ± 0.07
Density (g/mL)	1.0683 ± 0.0009	1.2461 ± 0.0008
HHV (MJ/kg)	22.328 ± 0.107	16.105 ± 0.769

[a] Calculated by difference: O (%) = 100 – C (%) – H (%) – Ashes (%).

The glycerol, methanol, and acetic acid content was quantified using an Agilent 7890 gas chromatograph equipped with a Flame Ionization Detector (FID) and a HP-FFAP Agilent 19091F- 105 capillary column. High purity glycerol (Sigma-Aldrich, ≥99.5 %, CAS: 56-81-5) was employed to prepare calibrate solutions.

Water composition was determined by Karl Fischer titration with a Mettler Toledo V20 KF Titrator and the ash content was quantified following the ISO 21656:2021. Density and pH were measured with a Mettler Toledo Densito 30PX and a Thermo Scientific Orion Star A215 pH/Conductivity Meter respectively. The High Heating Value (HHV) of crude and refined crude glycerol was determined in an IKA©-WERKE C2000 Basic Calorimeter, while the elemental analysis was performed in a Leco CHN 628 analyzer equipped with NDIR infrared cells.

The purification of crude glycerol increased the purity of refined crude glycerol up to 79.94 ± 2.43 % and significantly reduced the methanol content. The physical properties were modified after purification, and the density increased, while the high heating value (HHV) decreased. These properties are consistent with others reported in the literature [53,54]. The main impurities of refined crude glycerol were methanol, acetic acid, KOH, and residual free-fatty acids.

2.3. Catalyst characterization techniques

The properties of the fresh and spent catalysts were analyzed using several characterization techniques. The bulk chemical composition of the fresh catalyst was determined by inductively coupled plasma optical emission spectrometry (ICP-OES). The fresh and spent catalysts surface area (S_{BET}), pore volume (V_P), and pore size distribution were measured by N_2 adsorption-desorption using the BET and BJH methods, respectively. The crystalline phases of both fresh and spent catalysts were examined by X-ray diffraction (XRD), using the JCPDS database for identification. The crystallite size of some phases was calculated by the Scherrer's equation in the corresponding most intense peaks. The reducibility of the catalyst was assessed through hydrogen temperature-programmed reduction (H_2-TPR). The surface acidity of the reduced catalyst was quantified using temperature-programmed desorption of ammonia (TPD-NH_3). The surface morphology of the catalysts was analyzed using field emission scanning electron microscopy (FESEM) and the element dispersion by energy dispersive spectroscopy (EDS). The spent catalysts were subjected to elemental and thermogravimetric (TGA) analysis to determine the content and nature of the carbonaceous deposits formed during the reactions. The presence of potassium (K) on the catalyst surface was quantified by X-Ray Fluorescence (XRF) analysis performed on a sequential spectrometer (Thermo Fisher Scientific) equipped with a Rh X-ray tube. The Cu valence was analyzed by X-Ray Photoelectron Spectroscopy (XPS) by means of a Kratos Axis Supra equipment. Further details regarding the characterization techniques of the catalyst can be found in previous works [20,49].

2.4. Experimental setup and catalytic tests

Glycerol conversion was studied in a small laboratory-scale plant (PID Eng&Tech, Spain) operating at atmospheric pressure with a tubular quartz reactor (250 mm long and 9 mm internal diameter). In a typical experiment, the specified amount of catalyst was arranged between two layers of quartz wool on which 1 mL of inert sand (1.6 ± 0.2 g) was placed to preheat and vaporize the feed. Prior to the reaction, the catalyst was reduced at 300 °C under a 100 cm^3 STP min^{-1} flow of H_2 for 1 h. An electric furnace then heated the reactor to the specified reaction temperature using a PID controller that kept the temperature constant. A high-performance liquid chromatography (HPLC) pump introduces a 10 wt% aqueous solution of pure glycerol or refined crude glycerol through the top of the reactor with a flow rate of 0.1 mL min^{-1} accompanied by the corresponding flow of N_2, which serves as a carrier gas and as an internal standard for the online quantification of the gases produced in a gas chromatograph (Agilent 490) with thermal conductivity detectors (TCD). The liquid product stream was cooled and collected in an ice-bath condenser located at the outlet of the reactor and analyzed *offline* with a GC-FID (Agilent 7890 with an HP-FFAP Agilent 19091F-I05 column) using 1-butanol (PanReac, ≥99.5 %, CAS: 71-36-3) as the internal standard and glycerol (Sigma-Aldrich, ≥99.5 %, CAS: 56-81-5), methanol (Carlo Erba, ≥99.0 %, CAS: 67-56-1), acetic acid (Sigma-Aldrich, ≥99.0 %, CAS:64-19-7), 1,2-propanediol (Sigma-Aldrich, >99.0 %, CAS: 57-55-6), acetol (Sigma-Aldrich, >90 %, CAS: 116-09-6), acetaldehyde (Sigma-Aldrich, ≥99.5 %, CAS: 75-07-0), ethylene glycol (Labkem, >99.0 %, CAS: 107-21-1) and acetone (Carlo Erba, ≥99.9 %, CAS: 67-64-1) for quantification.

The total carbon of the liquid products was analyzed using a Shimadzu Total Organic Carbon Analyzer (TOC-L), and for all experiments, the carbon balance was greater than 94 %. More information about the experimental system can be found elsewhere [49].

2.5. Statistical analysis and evaluation

The influence of different operating conditions on the gas phase glycerol dehydration to acetol was studied for 2 h over a CuAl catalyst. The operational parameters analyzed were temperature (200–300 °C), W/m ratio (10–50 $g_{Catalyst}$ min $g^{-1}_{Glycerol}$), and carrier gas to liquid ratio (R_{GL}) (200–600 m^3_{Gas} STP $m^{3\,1}_{Liquid}$).

Firstly, the effects of two factors (temperature and W/m) were analyzed using a full factorial experimental design 2^k with three replicates at the center point to evaluate the experimental error and check whether the effects were linear. For that purpose, 7 experiments were performed (Table 2). The results were subjected to an analysis of variance (ANOVA) with 95 % confidence. The response variables were acetol yield and glycerol conversion. The statistical analysis results are shown as p-values and values below 0.05 indicate significant differences between the factors.

The best-performing conditions of the full factorial experimental design were used for the subsequent study of the effect of remaining operating conditions and for an extensive study of the catalyst stability during 52 h of time-on-stream. Moreover, these conditions were tested using refined crude glycerol to assess the impact of this feed on catalytic results for 2 and 29 h of time-on-stream.

Glycerol conversion (X_{Gly}) was calculated as:

$$X_{Gly}(\%) = \frac{moles\ of\ glycerol\ fed - moles\ of\ glycerol\ in\ the\ liquid\ products}{moles\ of\ glycerol\ fed} \cdot 100$$

Carbon yield to gases (CY_{Gas}) was determined as:

$$CY_{Gas}(\%) = \frac{moles\ of\ C\ in\ the\ gaseous\ products}{moles\ of\ C\ fed} \cdot 100$$

Carbon selectivity to liquid products (S_{Liquid}) was calculated as:

$$S_{Liquid_i}(\%) = \frac{moles\ of\ C\ in\ a\ liquid\ compound\ i}{\sum moles\ of\ C\ in\ the\ liquid\ products} \cdot 100$$

Table 2
Operating conditions of the experiments in actual values and codec factors.

Exp No.	Temperature (°C)	Codec factor	W/m ($g_{Catalyst}$ min $g^{-1}_{Glycerol}$)	Codec factor
1	300	1	50	1
2	250	0	30	0
3	200	−1	10	−1
4	200	−1	50	1
5	250	0	30	0
6	300	1	10	−1
7	250	0	30	0

3. Results and Discussion

3.1. Fresh catalyst characterization

3.1.1. Catalyst composition and textural properties

The chemical composition of the fresh calcined catalyst was determined by ICP-OES. The target copper content, expressed as Cu/(Cu + Al) (28.0 mol%), was satisfactorily achieved (28.4 mol%). The adsorption-desorption isotherms of N_2 and the pore size distribution of the fresh and reduced catalyst are shown in Fig. 1A and B, respectively.

The BET surface area (S_{BET}) of the calcined fresh CuAl catalyst was 225 $m^2\ g^{-1}$, and decreased marginally to 216 $m^2\ g^{-1}$ after the catalyst reduction with H_2. The pore volume (V_P) slightly increased from 0.40 to 0.43 $cm^3\ g^{-1}$ from the fresh to the reduced catalyst, while the mean pore size (d_P) remained constant at 6.73 nm in both samples. Fig. 1A shows very similar N_2 adsorption-desorption isotherms in the fresh and reduced catalyst. The catalysts show type IV(a) isotherms and H2(b) hysteresis cycles according to the IUPAC classification. This kind of isotherm are related to mesoporous materials with multilayer adsorption in a diverse range of neck sizes and shapes like inkbottle [55]. The pore size distribution is similar in both samples and pores are typically in the range of 2–20 nm, demonstrating that they are mesoporous materials. The textural properties of the calcined catalyst are consistent with those reported in the literature. A previous study [49] with a coprecipitated CuAl catalyst of 20 mol% of Cu and calcined at 675 °C generated a S_{BET} of 186 $m^2\ g^{-1}$, V_P of 0.40 $cm^3\ g^{-1}$, and d_P of 8.0 nm.

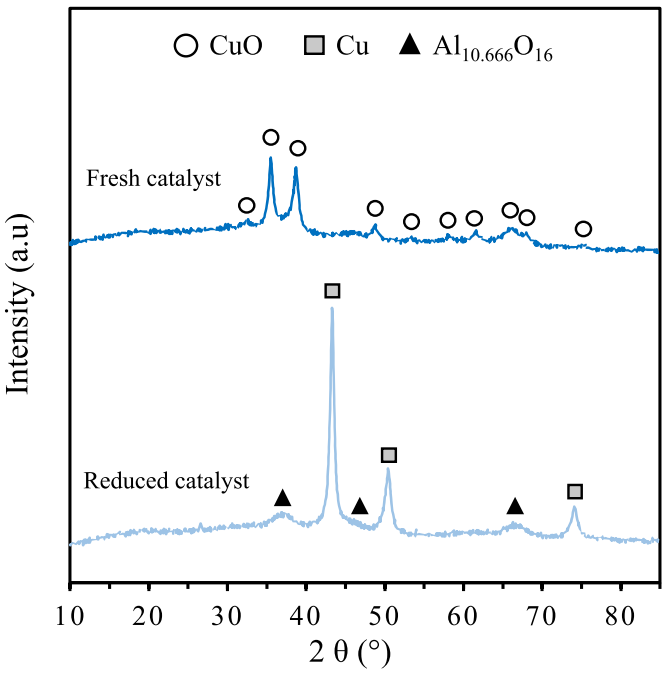

Fig. 2. XRD patterns of fresh and reduced CuAl catalyst.

3.1.2. XRD analysis

Fig. 2 shows the XRD patterns of the fresh and reduced CuAl catalyst. The fresh catalyst is poorly crystalline, and the only discernible peaks can be associated with the tenorite phase (CuO) (JCPDS 01-072-0629) at 2θ = 32.5, 35.6, 38.7, 48.8, 53.5, 58.1, 61.4, 66.5, 68.2, and 72.5°. The possible presence of alumina (Al_2O_3) was considered, but its characteristic peaks could not be recognized. This fact was also observed in other studies, like the one conducted by Mane et al. [57], where a Cu-Al catalyst was synthesized by coprecipitation with a 50 mol% of Cu, but no aluminum phase could be detected in the XRD patterns of the fresh catalyst.

During the reduction step, CuO is reduced to its metallic state (Cu^0), generating more crystalline diffractograms with defined peaks. The metallic copper phase (JCPDS 01-085-1326) was identified at the peaks 2θ = 43.3, 50.5, and 74.2° in the reduced catalyst XRD pattern. In addition, the presence of non-stoichiometric alumina $Al_{10.666}O_{16}$ (JCPDS 01-080-0956) was detected in the reduced catalyst at the diffraction peaks 2θ = 37.6, 46.9, and 67.2°. The disappearance of the copper oxide phase in the reduced catalyst states that the activation has been complete and satisfactory. The crystallite size of metallic Cu in the reduced catalyst was calculated using Scherrer's equation at the most intense characteristic peak at 2θ = 43.3°, showing a crystallite size of 15.1 nm.

3.1.3. Catalyst reducibility and acidity

The CuAl catalyst was analyzed using H_2-TPR to evaluate its reducibility (Fig. 3A). Two reduction peaks were observed at 219 °C (α) and 261 °C (β), corresponding to highly dispersed and bulk CuO, respectively. The larger α-peak area (62 %) suggests high CuO dispersion [56–58]. The reduction temperature selected was 300 °C.

The catalyst acidity plays a critical role in the dehydration of glycerol. Depending on the amount and strength of the acid sites, the glycerol molecule will be kinetically favored to produce acetol or acrolein. Weak acid sites (Lewis) favor the coordination of the primary hydroxyl group, polarizing the primary C-O bonds and resulting in acetol [59]. In addition, several studies have demonstrated that the presence of moderate acid sites also catalyzes glycerol dehydration [35]. Therefore, the presence of a large number of weak to moderate acid sites on the catalyst is necessary to promote acetol selectively. TPD-NH_3 analysis was performed for the study and quantification of the acid sites. The resulting

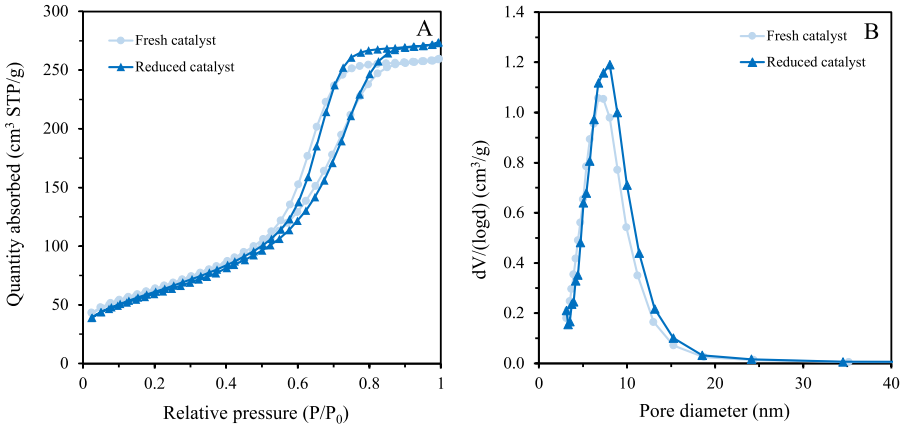

Fig. 1. N_2 adsorption-desorption isotherms of the fresh and reduced CuAl catalyst (A) and pore size distribution of the fresh and reduced CuAl catalyst (B). Reduction temperature: 300 °C.

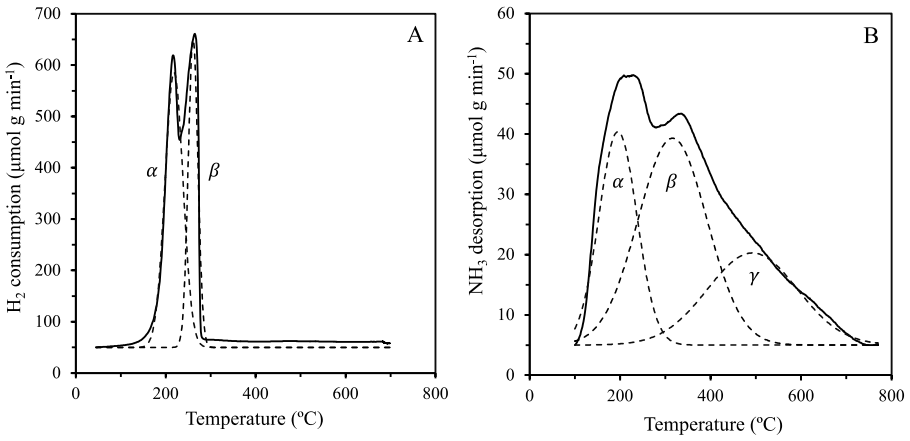

Fig. 3. H_2-TPR of the fresh (A) and NH_3-TPD of the reduced (B) CuAl catalyst.

desorption profile is displayed in Fig. 3B. The CuAl catalyst exhibited an acid site concentration of 1476.4 μmol NH_3 g^{-1}. The TPD profile was deconvoluted by Gaussian fitting in three different strength regions (α, β, and γ) according to the literature [60]. The α-peak represents the weak acid sites and is located at 195 °C, the β-peak characterizes the moderate acid sites at 316 °C, and the γ-peak denotes the strong acid sites at 493 °C. The weak and moderate acid sites are predominant, accounting for 24.4 and 46.6 % of the area respectively, while strong acid sites account for 27.0 % of the area. These results are consistent with those found in the literature on copper-aluminum coprecipitated catalysts [49,61], where acidity determined by NH_3-TPD varied from 1400 to 1600 μmol NH_3 g^{-1}. In these studies, CO_2-TPD analyses were carried out, and the presence of basic sites was minimal. Cu-based catalysts are known to exhibit Lewis acidity, with metallic copper acting as the active Lewis acid site [59]. In contrast, Brønsted acid sites (typically introduced by metals like W or Nb, or highly acidic supports such as zeolites) promote acrolein formation [38]. Since CuAl catalysts lack Brønsted acidity, glycerol dehydration is expected to proceed selectively via the Lewis acid pathway, favoring acetol over acrolein.

3.1.4. *FESEM and EDS*

The morphology and element dispersion of the fresh CuAl catalyst were analyzed by field emission scanning electron microscopy (FESEM) and energy dispersive spectroscopy (EDS). Fig. 4A shows a FESEM image and Fig. 4B–D the EDS mappings of Cu, Al, and O respectively.

The fresh catalyst has a rough surface with different morphologies and pores of diverse shapes heterogeneously distributed. The EDS mapping of copper (Fig. 4B) shows that the copper has distributed homogeneously over the entire surface, generating a high dispersion of copper oxide throughout the aluminum support (Fig. 4C). The active metal dispersion over the catalyst surface is crucial for good catalytic efficiency. Some authors reported that the synthesis of supported metal catalysts by the coprecipitation method favors the generation of uniform metal nanoparticles on the catalyst surface and enhances the interaction between metal oxides, generating catalysts with high catalytic activity [62,63].

Fig. 5 shows a closer FESEM image of the fresh catalyst. It can be observed that the surface is irregular and consists of a wide range of differently shaped pores. CuO was distributed throughout the surface and two types of particles could be distinguished: highly dispersed and bulk. The highly-dispersed copper was deposited on the support forming

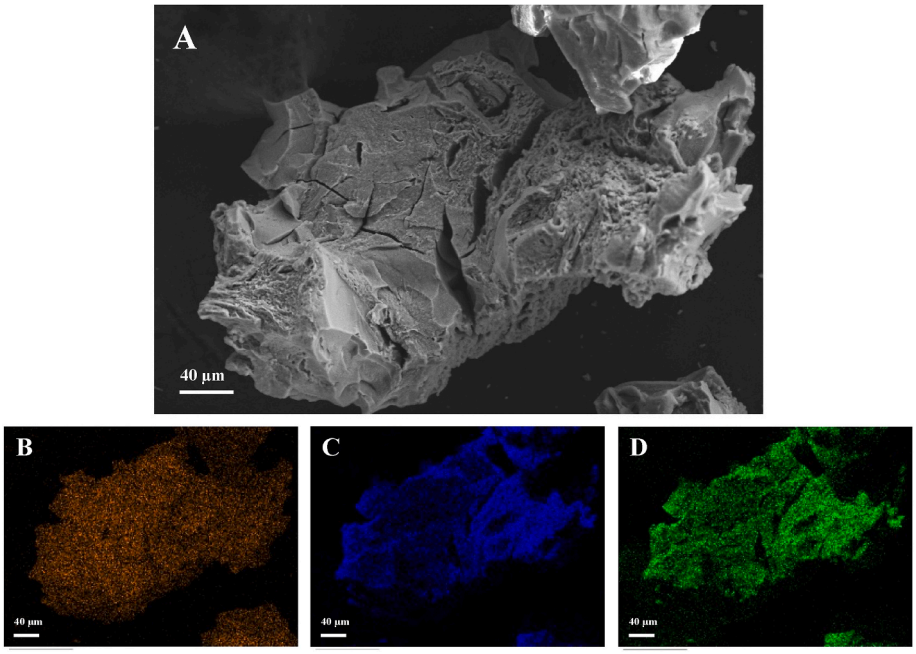

Fig. 4. FESEM image of fresh CuAl catalyst (A) and EDS mapping of copper (B), aluminum (C), and oxygen (D).

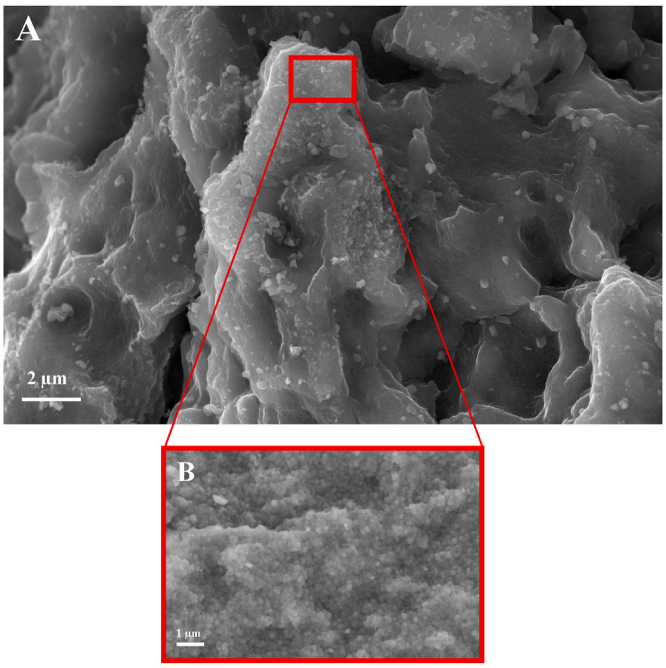

Fig. 5. FESEM images of the fresh CuAl catalyst surface.

small homogeneous particles (Fig. 5B), and bulk copper could be observed in the larger irregularly shaped particles due to the agglomeration of copper (Fig. 5A). These results confirm the TPR analysis conclusions, which proposed the presence of two types of copper particles that would be reduced at different temperatures due to their nature.

3.2. Catalytic studies

3.2.1. Influence of temperature and catalyst weight to glycerol mass flow ratio

The effect of reaction temperature (T) and W/m ratio was investigated through a full factorial experimental design where the temperature was varied from 200 to 300 °C and the W/m ratio from 10 to 50 $g_{Catalyst}$ min $g^{-1}_{Glycerol}$. The W/m ratio was adjusted by varying the catalyst loading from 0.1 to 0.5 g. The experiments were performed using a 10 wt % pure glycerol feed, a liquid feeding rate of 0.1 mL min^{-1}, and 20 cm^3 STP min^{-1} N_2 flow (R_{GL} of 200 m^3_{Gas} STP $m^{3\,1}_{Liquid}$) at atmospheric pressure. The influence of the operating conditions in the response variables is shown in Fig. 6 and the relative effects in terms of codec factors according to the ANOVA analysis are displayed in Table 3.

The results obtained from the statistical analysis of acetol yield (Fig. 6A) revealed a significant effect of temperature (p-value 0.007), W/m ratio (p-value 0.008), and the interaction between both factors (p-value 0.013). The interaction could be observed at high temperatures (300 °C), where the effect of W/m ratio was no longer significant, as the error bars of both points (10 and 50 $g_{Catalyst}$ min $g^{-1}_{Glycerol}$) overlapped. This phenomenon could be ascribed to the kinetics of reactions at elevated temperatures, as thermal energy allowed them to happen more easily regardless of the catalyst loading employed. In addition, the results showed a non-linear trend (p-value 0.003) in the studied area, and the factors created a maximum acetol yield at the central point. The temperature and W/m values that maximized acetol yield were 250 °C and 30 $g_{Catalyst}$ min $g^{-1}_{Glycerol}$, generating 464.7 ± 11.3 mg_{Acetol} $g^{-1}_{Glycerol}$ (59.6 % acetol selectivity) with a 95 % confidence level.

Similarly, the analysis of variance performed on the glycerol conversion response variable (Fig. 6B) has revealed a significant effect of temperature (p-value 0.016), W/m ratio (p-value 0.019), and interaction between the two factors (p-value 0.030). In the region located at higher temperatures, the effect of W/m ratio was not significant, while at lower temperatures (200 °C) it was. This interaction could again be associated with the thermodynamics of the reactions favored at higher temperatures. As with the acetol yield, the results show a non-linear trend (p-value 0.008) in the glycerol conversion, obtaining the highest conversion at 300 °C and 50 $g_{Catalyst}$ min $g^{-1}_{Glycerol}$ of the catalyst with 97.1 ± 2.0 %.

The operating conditions that maximized acetol yield were chosen for further investigation of the effects of other variables (250 °C and a W/m ratio of 30 $g_{Catalyst}$ min $g^{-1}_{Glycerol}$).

The dehydration reaction of glycerol to acetol has been studied in temperatures from 200 to 300 °C. The study of the effect of temperature is essential because a few degrees can significantly change product distribution and glycerol conversion. This fact has been reported in

Table 3
Relative effects of operating conditions on the response variables according to the ANOVA analysis.

Response variable	R^2	Constant	T	W/m	T·W/m	Central point
Acetol yield (mg_{Acetol} $g^{-1}_{Glycerol}$)	0.99	318.1	66.9	61.9	−48.6	146.6
Glycerol conversion (%)	1	73.5	21.9	11.4	−9.7	21.9

Response = Constant + Coefficient T · T + Coefficient W/m · W/m + Coefficient T·W/m · T·W/m + Coefficient central point · Central point.

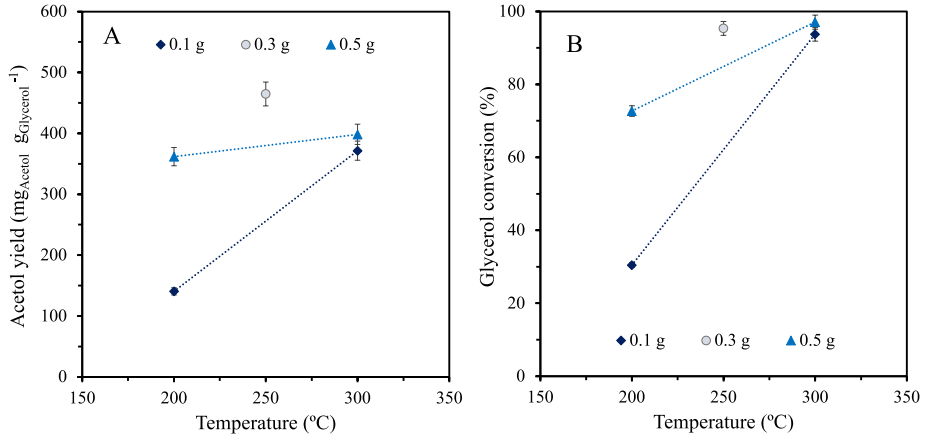

Fig. 6. Interaction plots between temperature and W/m ratio for acetol yield (A) and glycerol conversion (B). Reaction conditions: 1 bar, 10 wt% aqueous solution of pure glycerol, liquid feeding rate of 0.1 mL min^{-1}, and 20 cm^3 STP min^{-1} N_2 flow (R_{GL} of 200 m^3_{Gas} STP $m^{3\,1}_{Liquid}$).

several studies in the literature, such as the one carried out by Sato et al. [37]. They used an impregnated Cu/Al_2O_3 catalyst with a 30 wt% glycerol aqueous solution and a W/m of 55.55 $g_{Catalyst}$ min $g^{-1}_{Glycerol}$ and demonstrated that an increase in reaction temperature from 260 to 300 °C decreased acetol selectivity from 80 to 45 % and glycerol conversion from 100 to 55 %, mainly due to catalyst deactivation at higher temperatures. Correspondingly, Mazarío et al. [64] used coprecipitated Cu-Mg-Al mixed oxides for the selective dehydration of glycerol to acetol in the range of 220–280 °C. In that study, they used a 10 wt% glycerol solution in methanol and a W/m ratio of 150 $g_{Catalyst}$ min $g^{-1}_{Glycerol}$ and concluded that 240 °C was the best temperature.

The W/m ratio is an important parameter as the greater the catalyst amount, the larger the number of active sites, however, acetol selectivity can be modified. Basu et al. [28] studied the influence of varying the catalyst weight from 0.5 to 1.5 g in a batch reactor at 200 °C with a 20 vol% aqueous glycerol solution. The study revealed that increasing the catalyst loading positively influenced glycerol conversion, reaching 100 % conversion at 1.5 g. Conversely, if the catalyst loading was increased from 1 to 1.5 g, acetol selectivity decreased from 60 to 35 % due to the formation of several by-products.

From the full factorial design, it can be concluded that the best temperature and W/m conditions for the production of acetol were 250 °C and 30 $g_{Catalyst}$ min $g^{-1}_{Glycerol}$, with results of 464.7 ± 11.3 mg_{Acetol} $g^{-1}_{Glycerol}$ and a glycerol conversion of 95.4 ± 2.0 % with 95 % confidence. Under these operating conditions, the only gases produced were H_2 and CO_2 due to the high activity of copper towards the Water Gas Shift reaction. The volumetric composition (free of N_2 and H_2O) was 87.2 and 12.8 % of H_2 and CO_2 respectively. The carbon yield to gases was 1.02 ± 0.15 %, and 262.4 ± 49.3 $mmol_{H2}$ $mol^{-1}_{Glycerol}$ was produced. The main liquid by-products were ethylene glycol, acetic acid, and 1,2-PDO. In terms of coke deposition during the reaction, the elemental analysis detected 6.90 ± 0.55 wt% of C on the catalyst.

3.2.2. *Influence of carrier gas flow rate*

The influence of the R_{GL}, defined as the ratio between the carrier gas to liquid flow, was studied. For that purpose, the N_2 flow rate was set at 20, 40, or 60 cm^3 STP min^{-1}, to obtain a R_{GL} of 200, 400, or 600 m^3_{Gas} STP $m^{3\text{-}1}_{Liquid}$, respectively. The experiments were performed at 250 °C using a W/m ratio of 30 $g_{Catalyst}$ min $g^{-1}_{Glycerol}$, a 10 wt% glycerol feed solution, and a liquid feeding rate of 0.1 mL min^{-1} at atmospheric pressure. Fig. 7A shows the acetol yield and glycerol conversion results and Fig. 7B presents the carbon selectivity of the quantified reaction by-products.

The glycerol conversion remained unaffected by the variation of the R_{GL} and showed values around 95.4 %. On the contrary, a non-linear trend could be observed in acetol yield. There was a minimum production using a R_{GL} of 200 m^3_{Gas} STP $m^{3\text{-}1}_{Liquid}$, which increased with higher R_{GL} ratios. The acetol yield with a R_{GL} of 400 m^3_{Gas} STP $m^{3\text{-}1}_{Liquid}$ was 563.6 ± 17.0 mg_{Acetol} $g^{-1}_{Glycerol}$ (73.1 % acetol selectivity), while with a R_{GL} of 600 m^3_{Gas} STP $m^{3\text{-}1}_{Liquid}$, it was 531.5 ± 42.3 mg_{Acetol} $g^{-1}_{Glycerol}$ (68.4 % acetol selectivity). Since the error bars overlapped with R_{GL} of 400 and 600 m^3_{Gas} STP $m^{3\text{-}1}_{Liquid}$, the effect between these two values could not be considered significant. The use of higher N_2 flow rates would imply larger installations, which entails higher costs in both equipment and supplies as well as more energy to heat the N_2 for the reaction. To improve the economy and efficiency of the process, 40 cm^3 STP min^{-1} of N_2 (R_{GL} of 400 m^3_{Gas} STP $m^{3\text{-}1}_{Liquid}$) was selected as the most appropriate ratio.

Product selectivity to secondary products such as acetic acid, 1,2-PDO, or ethylene glycol decreased slightly by increasing the N_2 flow rate but remained at residual concentrations. Additionally, several unidentified products have been detected and were the lowest for a R_{GL} of 400 m^3_{Gas} STP $m^{3\text{-}1}_{Liquid}$. Table 4 presents the overall results corresponding to the gas product distribution and carbon deposits generated during the reactions. The increase in N_2 flow rate slightly increased the volumetric composition of H_2, thus decreasing the proportion of CO_2. Regarding the carbon yield to gas, it has slightly decreased from 1.02 ± 0.15 % to 0.87 ± 0.13 % from a R_{GL} of 200–600 m^3_{Gas} STP $m^{3\text{-}1}_{Liquid}$, generating a minimum with a 400 m^3_{Gas} STP $m^{3\text{-}1}_{Liquid}$, where the carbon yield to gas was 0.77 ± 0.01 %. In the same way, the H_2 yield decreased as the N_2 flow rate increased. The coke deposition during the reaction decreased slightly at higher R_{GL} ratios.

There is scarce information regarding the effect of carrier gas flow rate on the glycerol dehydration to acetol reaction. However, in the present work, it was shown to have a significant effect on acetol production. The same conversion was observed for the three R_{GL} ratios, however, acetol selectivity increased from 200 to 600 m^3_{Gas} STP $m^{3\text{-}1}_{Liquid}$. Additionally, the secondary product distribution slightly changed, and at higher R_{GL} ratios 1,2-PDO production decreased, which is generated from acetol hydrogenation. One possible explanation is that at higher N_2 flow rates, the produced H_2 is removed more rapidly from the catalyst

Table 4
Catalytic results of gases and solids from the N_2 flow rate experiments. Reaction conditions: 250 °C, 1 bar, 30 $g_{Catalyst}$ min $g^{-1}_{Glycerol}$, and a 0.1 mL min^{-1} flow rate of a 10 wt% aqueous solution of pure glycerol for 2 h.

R_{GL} (m^3_{Gas} STP $m^{3\text{-}1}_{Liquid}$)	200	400	600
Gas composition (%vol, N_2 and H_2O free)			
H_2	87.2 ± 1.8	89.4 ± 0.5	89.8 ± 0.1
CO_2	12.8 ± 1.8	10.6 ± 0.5	10.2 ± 0.1
Gas yields			
Carbon to gas (%)	1.02 ± 0.15	0.77 ± 0.01	0.87 ± 0.13
H_2 yield ($mmol_{H2}$ $mol_{Glycerol}^{-1}$)	262.4 ± 49.3	195.3 ± 7.7	203.8 ± 21.5
Solid yields			
C in catalyst (wt%)	6.90 ± 0.55	6.09 ± 0.09	6.10 ± 0.13

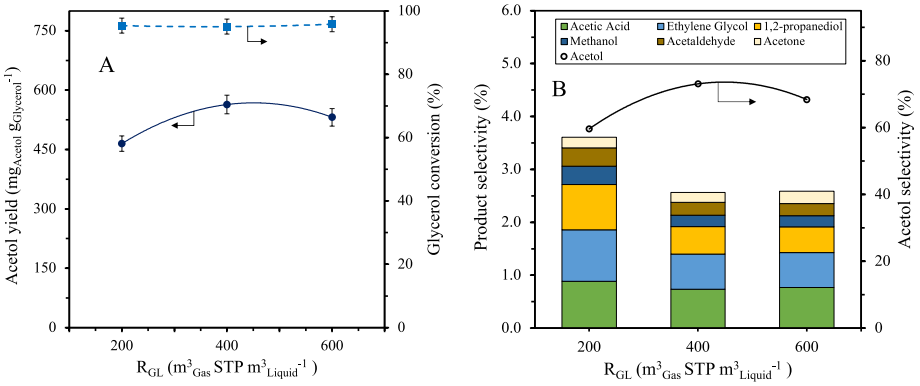

Fig. 7. Influence of R_{GL} on acetol yield and glycerol conversion (A) and product selectivity (B). Reaction conditions: 250 °C, 1 bar, 10 wt% aqueous solution of pure glycerol, and a W/m ratio of 30 $g_{Catalyst}$ min $g^{-1}_{Glycerol}$.

surface, thereby minimizing the acetol hydrogenation reaction to 1,2-PDO. Similarly, the produced acetol may also desorb from the surface more quickly as N_2 dilutes its concentration in the gas phase, reducing its likelihood of being re-adsorbed onto active sites and undergoing further transformation into secondary products or coke. Neira D'Angelo et al. [65] investigated the effect of R_{GL} ratios on the aqueous phase reforming of sorbitol. Their study demonstrated that the amount of N_2 played a crucial role in both sorbitol conversion and H_2 selectivity. At higher R_{GL} ratios, the removal of H_2 from the catalyst surface was enhanced, thereby minimizing secondary reactions and increasing selectivity. This effect was attributed to the reduction in H_2 partial pressure in the gas phase at higher R_{GL}, which, in turn, improved the overall mass transfer coefficient of H_2 in the gas phase from the solid surface.

From this study, it can be concluded that increasing the R_{GL} from 200 to 600 m^3_{Gas} STP m^{-3}_{Liquid} influenced the dehydration of glycerol to acetol. The effect of increasing the N_2 flow rate was positive as the amount of acetol generated improved substantially and the carbon yield to gas and coke deposition decreased. The most suitable N_2 flow rate was found at 40 cm^3 STP min^{-1} (R_{GL} of 400 m^3_{Gas} STP m^{-3}_{Liquid}) where there was a glycerol conversion of 95.1 ± 1.1 % and an acetol production of 563.6 ± 17.0 $mg_{Acetol}\ g^{-1}_{Glycerol}$.

3.2.3. Refined crude glycerol tests

The best operating conditions for acetol production deduced in the previous sections were further used for the study of the dehydration reaction of refined crude glycerol (RCG). The reaction conditions were 250 °C, 30 $g_{Catalyst}$ min g^{-1}_{RCG}, 40 cm^3 STP min^{-1} of N_2 (R_{GL} of 400 m^3_{Gas} STP m^{-3}_{Liquid}), and a 0.1 mL min^{-1} flow rate of a 10 wt% aqueous solution of refined crude glycerol for 2 h. Table 5 displays the effect of using pure glycerol or refined crude glycerol as feeding over the CuAl catalyst under the same operating conditions and Fig. 8 shows the carbon selectivity to liquid products. It should be noted that, as refined crude glycerol has a glycerol purity of almost 80 %, the W/m ratio increased slightly compared to the experiments carried out with pure glycerol up to 37.5 $g_{Catalyst}$ min $g^{-1}_{Glycerol}$.

The catalytic performance of refined crude glycerol was very similar to that obtained with pure glycerol. Glycerol conversion improved slightly from 95.1 to 98.7 % with refined crude glycerol, while acetol generation remained constant in both cases, demonstrating that the presence of impurities did not affect the catalytic performance during 2 h of experiment. The generation of liquid by-products increased in reactions with refined crude glycerol, but the products were found in residual concentrations. In addition, the presence of several unidentified products was detected.

Table 5
Catalytic results of refined crude glycerol experiments compared to those with pure glycerol for 2 h. Reaction conditions: 250 °C, 1 bar, R_{GL} of 400 m^3_{Gas} STP m^{-3}_{Liquid}, and a 0.1 mL min^{-1} flow rate of a 10 wt% aqueous solution of pure or refined crude glycerol for 2 h.

Experiment#	Refined crude glycerol	Pure glycerol
W/m	30 $g_{Catalyst}$ min g^{-1}_{RCG}	30 $g_{Catalyst}$ min $g^{-1}_{Glycerol}$
Liquid yields		
Acetol yield ($mg_{Acetol}\ g^{-1}_{Glycerol}$)	570.4 ± 13.4	563.6 ± 17.0
Glycerol conversion (%)	98.7 ± 0.9	95.1 ± 1.1
Gas composition (%vol, N_2 and H_2O free)		
H_2	86.3 ± 0.8	89.4 ± 0.5
CO_2	13.7 ± 0.8	10.6 ± 0.5
Gas yields		
Carbon to gas (%)	1.28 ± 0.14	0.77 ± 0.01
H_2 yield ($mmol_{H2}\ mol_{Glycerol}^{-1}$)	241.5 ± 10.3	195.3 ± 7.7
Solid yields		
C in catalyst (wt%)	5.75 ± 0.55	6.09 ± 0.09

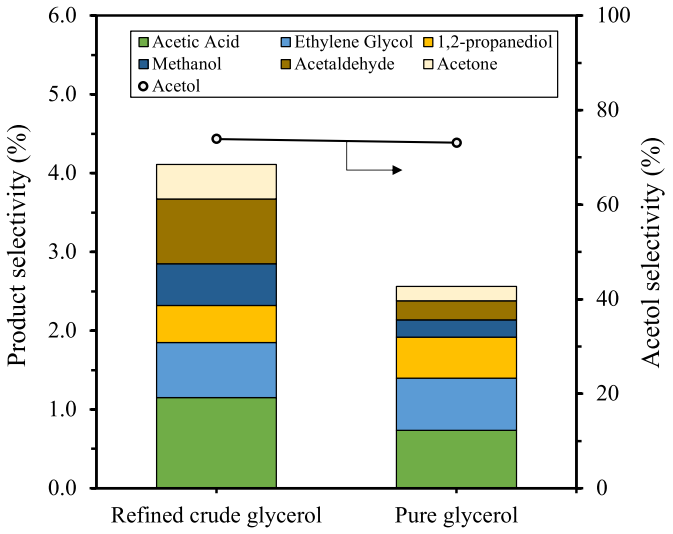

Fig. 8. Product selectivity of pure and refined crude glycerol for a TOS of 2 h. Reaction conditions: 250 °C, 1 bar, 10 wt% aqueous solution of pure or refined crude glycerol, 0.3 $g_{Catalyst}$, and 40 cm^3 STP min^{-1} of N_2 (R_{GL} of 400 m^3_{Gas} STP m^{-3}_{Liquid}).

The gas composition was similar using both feeds, but the carbon yield to gas increased slightly with the use of refined crude glycerol. Correspondingly, the H_2 yield was favored by refined crude glycerol and increased by 24 % up to 241.5 ± 10.3 $mmol_{H2}\ mol^{-1}_{Glycerol}$. In terms of solids formation, a similar generation of carbonaceous deposits was observed. The increase in H_2 production with refined crude glycerol in comparison to pure glycerol has been reported by other authors in crude glycerol reforming reactions [52,66,67]. These works suggest that the impurities present in crude glycerol, such as methanol or free-fatty acids, are responsible for the slight increase in the initial catalytic activity and H_2 yield under similar conditions, while the presence of KOH could favor the formation of carbonaceous deposits. Remón et al. [68] studied the effect of impurities in the steam reforming of biodiesel crude glycerol. They concluded that the presence of KOH increased the initial solid formation but had a catalytic impact on the gasification reactions of the carbon deposits, causing a decrease in the catalyst carbon content over time. This fact corroborates the trend observed in Table 5, where the carbon in the catalyst using refined crude glycerol was similar to that of pure glycerol but slightly increased carbon yield to gas.

These results are promising, as they demonstrate that under the same operating conditions, it was possible to produce renewable acetol and H_2 with slightly better catalytic results using refined crude glycerol similar to that generated as a by-product in the biodiesel industry.

3.3. Stability study

3.3.1. Pure glycerol

The catalytic activity of the CuAl catalyst was studied in a continuous reaction for 52 h. The operating conditions selected were 250 °C, 30 $g_{Catalyst}$ min $g^{-1}_{Glycerol}$, 0.1 mL min^{-1} of 10 wt% pure glycerol feed with two different N_2 flow rates: 20 or 40 cm^3 STP min^{-1}, R_{GL} of 200 or 400 m^3_{Gas} STP m^{-3}_{Liquid}, respectively. Fig. 9 shows the acetol yield (A) and the glycerol conversion (B) as a function of time-on-stream (TOS).

During the first few hours, both reactions followed the same trend and the yield to acetol reached a maximum of 547 and 526 $mg_{Acetol}\ g^{-1}_{Glycerol}$ for 200 and 400 m^3_{Gas} STP m^{-3}_{Liquid}, respectively for a TOS of 2.5 h. After that, there was a loss in catalytic activity and both the acetol yield and the glycerol conversion decreased, which was more pronounced at an N_2 flow rate of 20 cm^3 STP min^{-1} (200 m^3_{Gas} STP m^{-3}_{Liquid}) due to catalytic deactivation. As an example, from 2.5 to 23.5 h of TOS, yield to acetol decreased by 46 and 35 % for 20 and 40 cm^3 STP min^{-1},

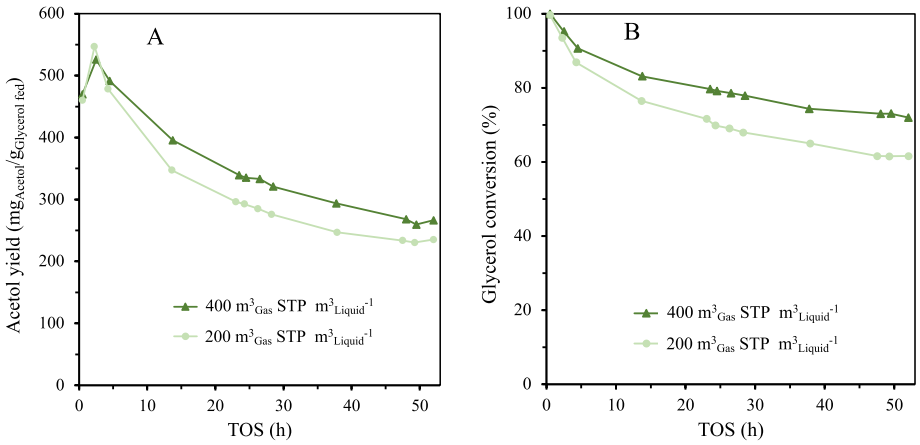

Fig. 9. Acetol yield (A) and glycerol conversion (B) as a function of time-on-stream (TOS) for pure glycerol stability study. Reaction conditions: 250 °C, 1 bar, 10 wt % aqueous solution of pure glycerol, and a W/m ratio of 30 $g_{Catalyst}$ min $g^{-1}_{Glycerol}$.

respectively, while glycerol conversion was reduced by 23 and 16 %, respectively. At longer TOS, both variables decreased to a lesser extent and tended to be balanced, with the reaction of 20 cm^3 STP min^{-1} of N_2 (200 m^3_{Gas} STP m^{3-1}_{Liquid}) stabilizing at 235 mg_{Acetol} $g^{-1}_{Glycerol}$ with a glycerol conversion of 61.6 % and the reaction of 40 cm^3 STP min^{-1} of N_2 (400 m^3_{Gas} STP m^{3-1}_{Liquid}) at 266 mg_{Acetol} $g^{-1}_{Glycerol}$ with a glycerol conversion of 72.0 % for a TOS of 52 h.

After the reactions, the spent catalysts were subjected to an elemental analysis that revealed a carbon content of 11.8 and 10.5 wt% for the reactions under 20 and 40 cm^3 STP min^{-1} respectively. These results are of great interest, since in the experiments carried out for 2 h, carbon deposition was 6.90 and 6.09 wt% for 200 and 400 m^3_{Gas} STP m^{3-1}_{Liquid} respectively. The reaction by-products followed a similar trend to the performance of acetol and their selectivity decreased to a greater extent in the first hours of reaction, stabilizing at the end. It should be noted that the selectivity to unidentified products increased over time.

The results obtained in this work for the CuAl catalyst for 52 h of continuous operation demonstrate better catalytic performance compared to the literature studies for copper-aluminum catalysts using a lower W/m ratio (Table 6). Morales et al. [21] studied the glycerol dehydration to acetol at 280 °C and reported that after only 5 h of reaction, their Cu/γ-Al_2O_3 catalyst rapidly deactivated and the glycerol conversion decreased from 90 to 10 %, as well as the acetol product selectivity, which also decreased from 60 to 35 %. The catalyst deactivation was attributed to the deposition of carbon on the catalyst surface. Braga et al. [57] reported a drop in glycerol conversion from 85 to 35 % in 5 h of reaction, while acetol selectivity remained at 90 % in their 7CuAl catalyst. Similarly, Mazarío et al. [64] reported that the activity of their 5.0 %Cu-HT-4 catalyst decreased sharply after 9 h. Glycerol conversion reached a maximum of 80 % at a TOS of 2 h and decreased to 50 % after 9 h while the selectivity to acetol remained constant at approximately 50 mol% during the last 6 h.

The drop in the catalytic activity of Cu-based catalysts is a widespread problem and several authors have reported the catalyst deactivation due to different factors. In the case of glycerol dehydration, the main reason is carbon deposition, because the dehydration route favors the generation of carbonaceous deposits in the acidic sites, which block pores and reduce the number of available active sites [69,70]. Another reason for the deactivation of copper catalysts is the thermal sintering of Cu particles, forming inactive phases that drastically reduce catalytic activity [71,72]. Velasquez et al. [22] proposed using La_2O_3 as a basic support for Cu to enhance catalytic activity and prevent deactivation due to carbon deposition in acidic sites. A stable catalyst was achieved for a 20-h reaction with a 20 vol % aqueous glycerol feed at 260 °C with an acetol yield of 75 % (around 600 mg_{Acetol} $g^{-1}_{Glycerol}$). However, the use of lanthanum in catalysts drastically increases their cost.

3.3.2. *Refined crude glycerol*

The stability study was carried out with the refined crude glycerol under operating conditions of 250 °C, 30 $g_{Catalyst}$ min g^{-1}_{RCG}, R_{GL} of 400 m^3_{Gas} STP m^{3-1}_{Liquid}, and 0.1 mL min^{-1} of an aqueous solution of 10 wt% refined crude glycerol. The acetol yield and glycerol conversion were studied as a function of time-on-stream (TOS) for 29 h.

As displayed in Fig. 10, the catalytic activity of the CuAl catalyst for refined crude glycerol followed the same trend as that performed with pure glycerol in the first 5 h and a maximum peak of acetol yield, 561 mg_{Acetol} $g^{-1}_{Glycerol}$ was achieved with more than 91 % glycerol conversion for a TOS of 2.5 h. After that, the glycerol conversion and the acetol yield decreased extremely, demonstrating that there was a huge catalyst deactivation during the next few hours of the reaction. However, after the first 20 h of reaction, the system stabilized with a glycerol conversion of 9.9 % and an acetol yield of 50 mg_{Acetol} $g^{-1}_{Glycerol}$. At a TOS of 29 h, the reaction had to be stopped due to the overpressure generated by the plugging of the catalyst caused by the formation of solids.

Konaka et al. [73] reported that crude glycerol with impurities similar to those in the present study led to the deactivation of their Zr-Fe catalyst due to K deposition on the catalyst surface. They concluded that

Table 6
Comparison of long-term reaction results with other Cu-based catalysts from literature.

Catalyst	Reaction conditions and catalyst properties				Catalytic results						Ref.
	Temperature (°C)	W/m ($g_{Catalyst}$ min $g^{-1}_{Glycerol}$)	Feed (wt%)[a]	Cu loading	TOS (h)	$X_{Glycerol}$ (%)	S_{Acetol} (%)	TOS (h)	$X_{Glycerol}$ (%)	S_{Acetol} (%)	
Cu/Al_2O_3	280	38	6.2	10 wt%	1	90	60	5	10	35	[20]
7CuAl	250	67	10	6.75 wt%	1	85	90	5	35	90	[58]
5.0%Cu-HT-4	240	150	10[b]	4.9 wt%	2	80	45	9	50	50	[65]
CuAl	250	30	10	28 mol%	2	95	73	52	72	46	Present work

[a] wt% of glycerol in aqueous solution, unless other indicated.
[b] wt% of glycerol in methanol solution.

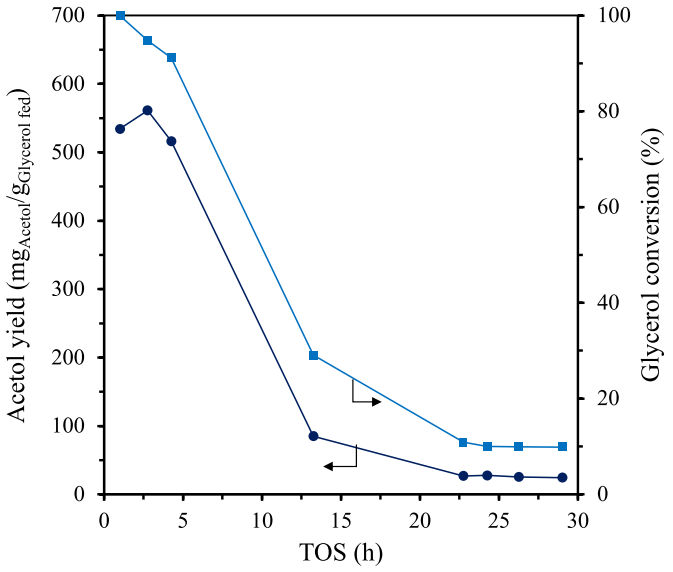

Fig. 10. Acetol yield and glycerol conversion as a function of time-on-stream (TOS) for refined crude glycerol stability study. Reaction condition: 250 °C, 1 bar, 10 wt% aqueous solution of refined crude glycerol, 400 m^3_{Gas} STP m^{-3}_{Liquid}, and a W/m ratio of 30 $g_{Catalyst}$ min g^{-1}_{RCG}.

the adhesion of K inhibited glycerol dehydration reactions by reducing the acidity of the catalyst over time. Similarly, Rajkhowa et al. [74] conducted a study with model impurities of crude glycerol derived from biodiesel production to assess the leading factors of Cu catalyst deactivation in glycerol hydrogenolysis. They evaluated the effect of glycerides (residual mono-, di- or triglyceride molecules from the transesterification), and KOH. They found that the glyceride molecules physically blocked the active sites, leading to a decrease in catalytic activity over time.

Sereshki et al. [75] evaluated the effect of salts present in crude glycerol (5 wt% NaCl) on catalysts in a fluidized bed reactor. In the study, it was shown that more than 99.8 % of the salts of crude glycerol were deposited on the catalyst surface forming crystals. As a consequence, the size of the particles increased markedly and bridges between particles were formed, blocking the active sites and deactivating the catalyst. However, the fluidized bed could be used as a preliminary step to remove salts and preserve the catalyst performance in the catalytic reactor.

3.4. Spent catalyst characterization

The spent catalysts were analyzed to evaluate the changes produced during the reactions. The catalysts selected for characterization were those used with the conditions that maximized acetol production (250 °C, 30 $g_{Catalyst}$ min $g^{-1}_{Glycerol}$, 0.1 mL min^{-1} of 10 wt% glycerol, and a R_{GL} of 400 m^3_{Gas} STP m^{-3}_{Liquid} with pure and refined crude glycerol for a TOS of 2 h, as well as the one used in the stability study with pure glycerol and a R_{GL} of 400 m^3_{Gas} STP m^{-3}_{Liquid} for a TOS of 52 h. The catalyst employed in the stability study with refined crude glycerol could not be characterized due to agglomeration produced during the reaction.

3.4.1. Textural properties

The textural properties of the spent catalysts are shown in Table 7, and the N_2 adsorption-desorption isotherms and pore size distribution are exhibited in Fig. 11. The S_{BET} of the catalyst after 2 h of reaction using pure glycerol increased slightly with respect to the reduced catalyst, while it decreased with the use of refined crude glycerol. After 52 h of reaction, the S_{BET} of the catalyst decreased by 12 % compared to the reduced catalyst, indicating a little variation. V_P decreased in all cases, more significantly in the long-term reaction, where it decreased by 41 % compared to the reduced catalyst. However, the d_P was similar for the two reactions with pure glycerol, which could indicate that after 52 h of reaction, the carbonaceous deposits did not form uniformly within the pores and only some were completely plugged, reducing the V_P. The isotherms of the spent catalysts showed no significant deviations compared to the fresh catalysts and manifested characteristics of mesoporous materials, displaying a hysteresis loop indicative of irregular pore structures of varying sizes.

Table 7
Textural and structural parameters of the spent CuAl catalysts.

Feed	Reaction time (h)	S_{BET} (m^2 g^{-1})	V_P (cm^3 g^{-1})	d_P (nm)	D_{Cu} (nm)
Pure glycerol	2	220	0.36	5.79	14.6
Refined crude glycerol	2	205	0.32	6.22	14.2
Pure glycerol	52	190	0.25	5.79	15.4

3.4.2. XRD analysis

XRD patterns of the spent catalysts are displayed in Fig. 12. It can be observed that the XRD profiles did not change with respect to the reduced catalyst in any of the reactions, and the same phases were detected. The only Cu phase was metallic copper, indicating that no bulk oxidation occurred during the reaction, even after a TOS of 52 h. In addition, the presence of silica (SiO_2) (JCPDS 01-085-0335) was detected in the reaction with refined crude glycerol due to cross-contamination of the catalyst with the silica bed.

The average crystallite sizes of metallic copper were calculated using the Scherrer equation for the most intense peaks located at $2\theta = 43.3°$, and are shown in Table 7. The Cu crystallite size showed a small increase from 14.6 nm after 2 h of reaction to 15.4 nm after 52 h of reaction with pure glycerol. These results could indicate that the sintering of copper is not a relevant cause of catalyst deactivation.

3.4.3. XPS analysis

To investigate the oxidation state of copper in the spent catalysts' surface, XPS analysis was performed to complement the XRD results. The Cu LMM Auger spectra of the spent catalysts after a TOS of 2 and 52 h were deconvoluted and are presented in Fig. 13, while the relative contributions of Cu species are summarized in Table 8.

The XPS spectra revealed the presence of Cu^0, Cu^+, and Cu^{2+} species, consistent with previously reported assignments [76,77], confirming partial surface oxidation. Notably, the relative area corresponding to Cu^0 remained constant at approximately 55 % for both TOS, indicating that the active phase is preserved over time and that no significant surface deactivation due to Cu^0 loss occurred. This stability is likely maintained by the reducing environment created by in situ hydrogen generation during the reaction, which could continuously shift the copper redox equilibrium. However, a slight increase in Cu^+ content was observed from 2 to 52 h of reaction, suggesting a progressive reduction of Cu^{2+} to Cu^+.

3.4.4. FESEM images

The spent catalysts were analyzed using FESEM to assess the morphological changes undergone during the reactions. The FESEM images of the reduced and spent catalysts are shown in Fig. 14. The metallic copper particles of the reduced catalyst (Fig. 14A) were homogeneously distributed over the surface and showed different sizes. After the reactions, larger particles could be observed, especially in the reaction with pure glycerol for a TOS of 52 h (Fig. 14D). This phenomenon is usually attributed to the thermal sintering of copper during reactions [71,72]. Increasing the size of the copper particles reduces the number of active sites and the dispersion of copper on the catalyst surfaces, which decreases their catalytic activity. However, the XRD analysis revealed that the crystallite copper size in the 52-h reaction did not

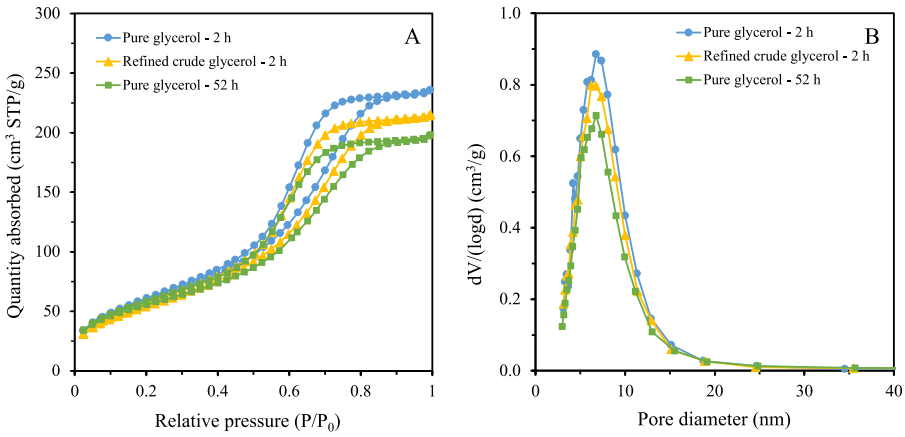

Fig. 11. N_2 adsorption-desorption isotherms (A) and pore size distributions (B) of spent CuAl catalysts.

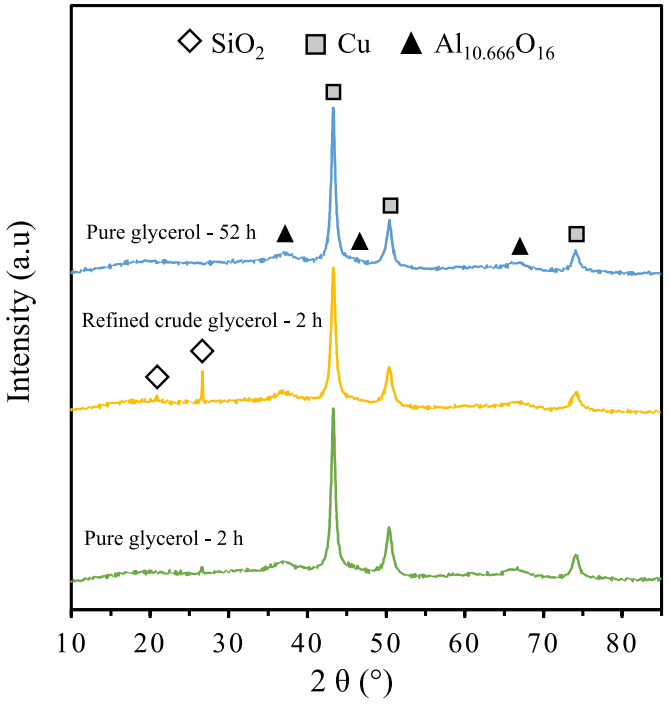

Fig. 12. XRD patterns of spent CuAl catalysts.

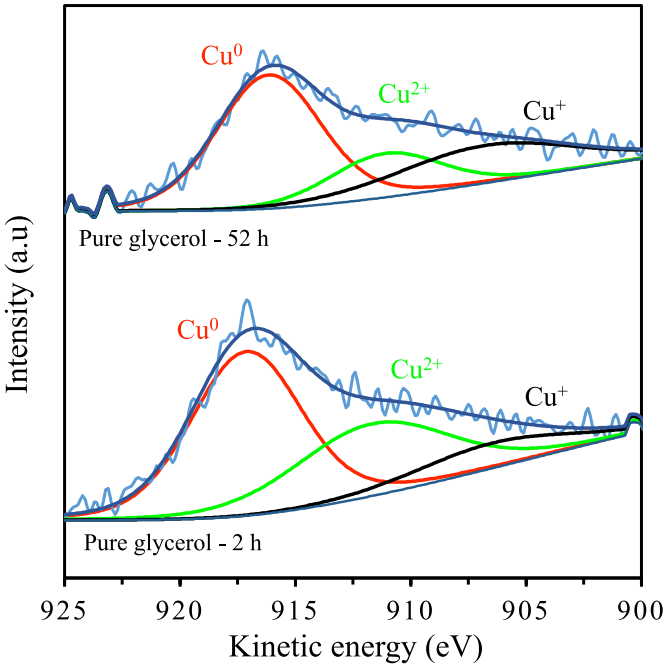

Fig. 13. XPS Cu LMM Auger spectra of spent catalysts.

increase extensively with respect to the 2-h experiments, demonstrating that copper sintering was not a determining factor in the catalyst deactivation.

3.4.5. *Catalyst deactivation by carbon and solid deposits*

The carbonaceous deposits of the spent catalysts used with pure glycerol at a TOS of 2 and 52 h were characterized using thermogravimetric analysis (TGA) in an oxidizing atmosphere. As a preliminary step, the samples underwent a degasification to remove water and possible reaction products adsorbed on the catalyst surface under an inert atmosphere of N_2 at 270 °C for 1 h. The oxidation of the carbonaceous deposits was carried out with 5 % O_2 in N_2 at a heating rate of 10 °C min^{-1} from 100 to 900 °C. Variations in sample weight during the analysis indicate the oxidation and volatilization of carbon species. The weight loss obtained from the derivation of the sample's TGA curves is presented in Fig. 15.

The graphs showed an increase in the amount of coke in the reaction at a TOS of 52 h. The values of weight loss determined by TGA were 5.40 and 9.01 wt% for a TOS of 2 and 52 h, respectively. This fact is consistent

Table 8
Surface distribution of Cu species determined by XPS Cu LMM Auger spectra in the spent catalysts.

Catalyst	Cu^0 (%)	Cu^+ (%)	Cu^{2+} (%)
Pure glycerol – 2 h	54.5	12.0	33.5
Pure glycerol – 52 h	54.6	26.3	19.1

with the elemental analysis, which revealed that the carbon content increased from 6.09 to 10.5 wt% from a TOS of 2–52 h, respectively. This trend was reported by Park et al. [78] using a mesoporous zeolite catalyst for the glycerol dehydration to acrolein. For a TOS of 2 h, the carbon content was 5.37 wt% and increased to 9.18 wt% for a TOS of 45 h, showing a reduced coke formation rate.

To assess the nature of coke, the graphs were deconvoluted by Gaussian fitting into three different curves (α, β, and γ). The α curve, observed in the 200 to 400 °C range, indicates the presence of coke precursors that oxidize at low temperatures and are linked to polymeric compounds derived from glycerol polymerization or acetylation, which adhere to the mesopores of the catalysts [79,80]. The β curve, with its

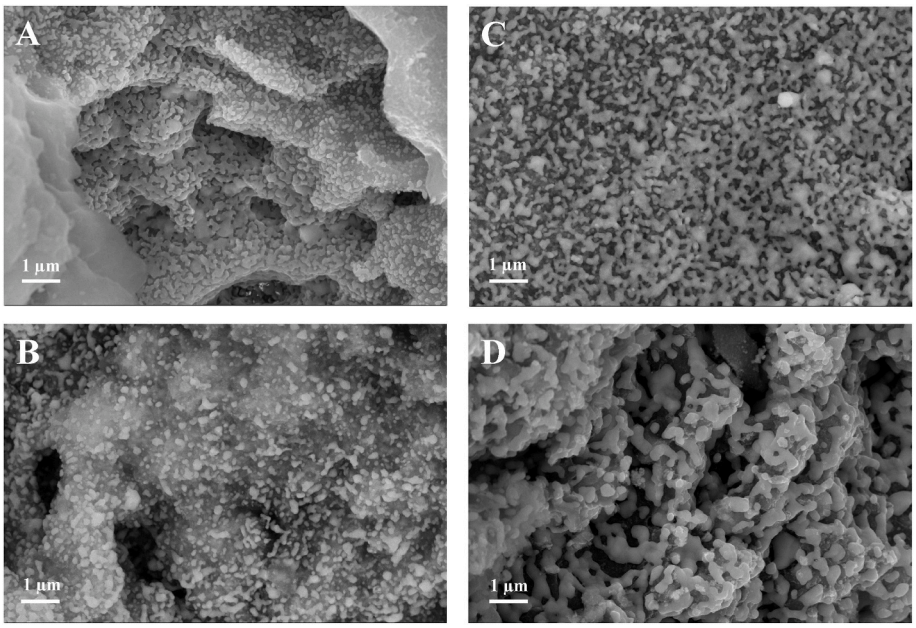

Fig. 14. FESEM images of reduced (A), spent with pure glycerol at TOS of 2 h (B), spent with refined crude glycerol at TOS of 2 h (C), and spent with pure glycerol at TOS of 52 h (D) CuAl catalysts.

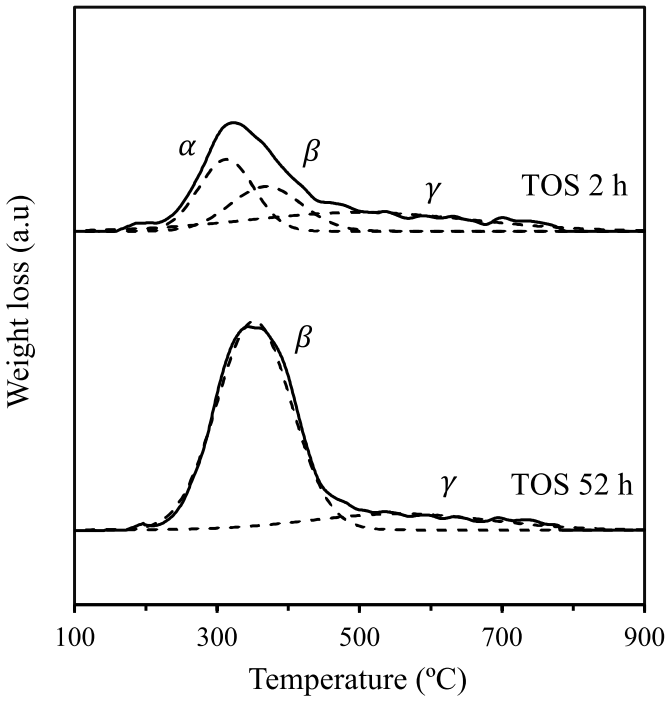

Fig. 15. Weight loss of the spent catalyst used with pure glycerol for a TOS of 2 and 52 h.

peak centered around 375 °C, is associated with the development of aromatization reactions that produce aromatic compounds that are oxidized at higher temperatures [78]. The γ curve appears at temperatures above 500 °C and corresponds to coke species that are difficult to oxidize, such as carbon nanotubes (CNTs), carbon nanofibers (CNFs), fullerenes, or graphitic carbon [81,82].

There was a transformation in the nature of carbon deposits during the reaction. For a TOS of 2 h, the α and β curves exhibited similar areas and corresponded to the oxidation of polymeric and aromatic compounds respectively. The γ curve, associated with coke species, exhibited the largest integrated area (37 %) and displayed a broad distribution from 400 to 800 °C. When the TOS increased to 52 h, the α curve shifted to higher temperatures and merged with the β curve, which indicated a reduction in polymeric compounds and an increase in aromatization reactions, resulting in a larger β curve. Meanwhile, the γ curve remained unchanged from a TOS of 2 and 52 h. This stability suggests that the formation of coke compounds that are difficult to oxidize does not increase with reaction time and is not favored under the studied reaction conditions.

According to Catuzo et al. [83], carbonaceous deposits impact glycerol dehydration by blocking active sites and limiting mass transfer. Polyglycol-type species, formed via polymerization or acetylation, mainly cover the external surface, causing initial deactivation. Aromatic compounds can penetrate the pore network, gradually clogging internal sites. Lastly, condensed coke forms deep within the pores and is highly resistant to oxidation, leading to more permanent deactivation by obstructing diffusion and access to active sites. In our study, a similar trend may have occurred. At a TOS of 2 h, polymeric species began to form on the external surface, as shown by the TGA under oxidizing conditions. After 52 h of TOS, these diminished, giving way to more stable aromatic compounds. These species may accumulate within the pore network, blocking internal active sites and contributing to the gradual catalyst deactivation. This hypothesis is further supported by BET analysis, which showed a decrease in both surface area and pore volume from 2 to 52 h, suggesting progressive pore blockage by carbonaceous residues.

Lauriol-Garbay et al. [84] conducted a deactivation study on the glycerol dehydration to acrolein over zeolites, showing that strong acid sites favor the formation of carbonaceous deposits, whereas Lewis acids are less prone to carbon deposition. This could explain why coke formation was not constant and was greater for shorter TOS. At the beginning of the reaction, the strong acid sites of the catalyst may quickly generate carbonaceous deposits, and as the reaction progresses, coke may start to deposit on the Lewis acid sites, but at a slower rate.

To evaluate solid deposition on the catalyst surface when using refined crude glycerol as feedstock, XRF analysis was carried out, revealing the presence of 1.5 wt% K on the surface of the spent catalyst after a TOS of 2 h. This suggests the incorporation of K as an impurity from the feed. According to the literature, K is known to negatively

impact catalytic performance by depositing on the surface of the catalyst, potentially blocking active sites and obstructing the pore structure [73]. However, in the long-term experiment (TOS = 29 h), the spent catalyst could not be recovered due to severe blockage from solid deposits, preventing further analysis. Although the K content at long reaction time could not be determined, it is plausible that K accumulation increased over time and may have contributed to catalyst deactivation and pore obstruction, together with the carbon deposition.

One potential method to recover catalyst performance is oxidative regeneration to remove carbon deposits, which were identified as the main cause of deactivation. Previous research on Cu-based catalysts has shown that O_2 treatment at 400–500 °C can effectively eliminate coke without compromising Cu dispersion or textural properties, as evidenced by consistent surface area and pore volume values before and after regeneration [85,86]. In our case, TGA under oxidizing conditions (Fig. 15) revealed that most carbon species were oxidized at 450 °C, suggesting this temperature as suitable for regeneration. Nevertheless, more experimental work is required to confirm the structural and catalytic stability of the material after treatment.

4. Conclusions

A copper-aluminum catalyst was synthesized by the coprecipitation method to study the effect of three operating conditions (temperature, catalyst weight to glycerol mass flow ratio, and carrier gas to liquid flow ratio) for the catalytic conversion of pure and refined crude glycerol to acetol. The physicochemical characterization showed a large dispersion of metallic copper with small crystallites (<15 nm) homogeneously distributed on the mesoporous surface of the reduced catalyst.

The results revealed that the operating parameters followed non-linear trends. The better conditions were 250 °C, a W/m ratio of 30 $g_{Catalyst}$ min $g^{-1}_{Glycerol}$, and a R_{GL} ratio of 400 m^3_{Gas} STP $m^{-3.1}_{Liquid}$. Under the best conditions and at a TOS of 2 h, the pure and refined crude glycerol reactions showed similar catalytic results (≈567 mg_{Acetol} $g^{-1}_{Glycerol}$ and a glycerol conversion >95 %). However, stability studies revealed that the use of refined crude glycerol completely deactivated the catalyst over time due to the formation of solids on the surface. On the other hand, pure glycerol had a better performance, and after 52 h of reaction, good stability was observed with a glycerol conversion of 72 % and 266 mg_{Acetol} $g^{-1}_{Glycerol}$.

XRD and XPS analysis of the spent catalysts identified only the presence of metallic copper phase in the bulk and a stable surface composition, demonstrating high catalytic stability even after a TOS of 52 h. The TGA results in oxidizing atmosphere demonstrated that the nature of the coke changed during the reaction. In the initial hours, the carbon deposition was greater, possibly due to the blockage of strong acidic active sites. Over time, carbon species transformed into less reactive carbonaceous compounds.

In this study, we generated outstanding catalytic results compared to those documented in existing literature, despite employing a significantly lower W/m ratio (30 $g_{Catalyst}$ min $g^{-1}_{Glycerol}$). Furthermore, the use of refined crude glycerol proved to be effective in the dehydration of glycerol to acetol. However, more studies are needed to minimize catalyst deactivation, particularly when using refined crude glycerol, in order to scale up the process.

CRediT authorship contribution statement

Alejandro Lete: Writing – original draft, Visualization, Validation, Methodology, Investigation, Formal analysis, Conceptualization. **Lucía García:** Writing – review & editing, Supervision, Project administration, Methodology, Funding acquisition, Conceptualization. **Joaquín Ruiz:** Writing – review & editing, Visualization, Funding acquisition. **Jesús Arauzo:** Writing – review & editing, Supervision, Funding acquisition.

Acknowledgements

The authors wish to express their gratitude to Project PID2020-114985RB-I00 funded by MICIU/AEI/10.13039/501100011033 and Aragón Government (Research Group Ref. T22_23R) for providing frame support for this work. Authors would like to acknowledge the use of Servicio General de Apoyo a la Investigación-SAI, Universidad de Zaragoza.

Data availability

Data will be made available on request.

References

[1] I.A.T.A. (IATA), Resolution on the industry's commitment to reach net zero carbon emissions by 2050 Boston (2021).
[2] I.C.A. Organization, Resolutions adopted at the 41st session of the assembly (2022). Montréal.
[3] D. Verma, R. Kumar, B. Rana, A. Sinha, Aviation fuel production from lipids by a single-step route using hierarchical mesoporous zeolites, Energy Environ. Sci. 4 (5) (2011) 1667–1671, https://doi.org/10.1039/c0ee00744g.
[4] E. Corporan, T. Edwards, L. Shafer, M. DeWitt, C. Klingshirn, S. Zabarnick, Z. West, R. Striebich, J. Graham, J. Klein, Chemical, thermal stability, seal swell, and emissions studies of alternative jet fuels, Energy Fuel. 25 (3) (2011) 955–966, https://doi.org/10.1021/ef101520v.
[5] M. Pearlson, C. Wollersheim, J. Hileman, A techno-economic review of hydroprocessed renewable esters and fatty acids for jet fuel production, Biofuels Bioprod. Bioref. Biofpr 7 (1) (2013) 89–96, https://doi.org/10.1002/bbb.1378.
[6] J. Serrano-Ruiz, E. Ramos-Fernandez, A. Sepulveda-Escribano, From biodiesel and bioethanol to liquid hydrocarbon fuels: new hydrotreating and advanced microbial technologies, Energy Environ. Sci. 5 (2) (2012) 5638–5652, https://doi.org/10.1039/c1ee02418c.
[7] A. Sutton, J. Kim, R. Wu, C. Hoyt, D. Kimball, L. Silks, J. Gordon, The conversion of starch and sugars into branched C_{10} and C_{11} hydrocarbons, ChemSusChem 9 (17) (2016) 2298–2300, https://doi.org/10.1002/cssc.201600669.
[8] M. Diaz-Perez, J. Serrano-Ruiz, Catalytic production of jet fuels from biomass, Molecules 25 (4) (2020), https://doi.org/10.3390/molecules25040802.
[9] R. West, Z. Liu, M. Peter, C. Gartner, J. Dumesic, Carbon-carbon bond formation for biomass-derived furfurals and ketones by aldol condensation in a biphasic system, J. Mol. Catal. Chem. 296 (1–2) (2008) 18–27, https://doi.org/10.1016/j.molcata.2008.09.001.
[10] M. Climent, A. Corma, S. Iborra, Conversion of biomass platform molecules into fuel additives and liquid hydrocarbon fuels, Green Chem. 16 (2) (2014) 516–547, https://doi.org/10.1039/c3gc41492b.
[11] S. Basu, A. Sen, A review on catalytic dehydration of glycerol to acetol, ChemBioEng Rev. 8 (6) (2021) 633–653, https://doi.org/10.1002/cben.202100009.
[12] S. Chozhavendhan, R. Kumar, S. Elavazhagan, B. Barathiraja, M. Jayakumar, S. Varjani, R. Singhania, R. Agarwal, R. Sukumaran, Utilization of Crude Glycerol from Biodiesel Industry for the Production of Value-Added Bioproducts (2018) 65–82, https://doi.org/10.1007/978-981-10-7431-8_4. Waste To Wealth.
[13] M. Checa, S. Nogales-Delgado, V. Montes, J. Encinar, Recent advances in glycerol catalytic valorization: a review, Catalysts 10 (11) (2020), https://doi.org/10.3390/catal10111279.
[14] M. Mohamad, R. Awang, W. Yunus, A review of acetol: application and production, Am. J. Appl. Sci. 8 (11) (2011) 1135–1139, https://doi.org/10.3844/ajassp.2011.1135.1139.
[15] J. Callison, N. Subramanian, S. Rogers, A. Chutia, D. Gianolio, C. Catlow, P. Wells, N. Dimitratos, Directed aqueous-phase reforming of glycerol through tailored platinum nanoparticles, Appl. Catal. B Environ. 238 (2018) 618–628, https://doi.org/10.1016/j.apcatb.2018.07.008.
[16] A. Morales-Marin, J. Ayastuy, U. Iriarte-Velasco, M. Gutierrez-Ortiz, C. T. Environm, Nickel aluminate spinel-derived catalysts for the aqueous phase reforming of glycerol: effect of reduction temperature, Appl. Catal. B Environ. 244 (2019) 931–945, https://doi.org/10.1016/j.apcatb.2018.12.020.
[17] G. Wen, Y. Xu, H. Ma, Z. Xu, Z. Tian, Production of hydrogen by aqueous-phase reforming of glycerol, Int. J. Hydrogen Energy 33 (22) (2008) 6657–6666, https://doi.org/10.1016/j.ijhydene.2008.07.072.
[18] F. Cai, D. Pan, J. Ibrahim, J. Zhang, G. Xiao, Hydrogenolysis of glycerol over supported bimetallic Ni/Cu catalysts with and without external hydrogen addition in a fixed-bed flow reactor, Appl. Catal. Gen. 564 (2018) 172–182, https://doi.org/10.1016/j.apcata.2018.07.029.
[19] I. Freitas, R. Manfro, M. Souza, Hydrogenolysis of glycerol to propylene glycol in continuous system without hydrogen addition over Cu-Ni catalysts, Appl. Catal. B Environ. 220 (2018) 31–41, https://doi.org/10.1016/j.apcatb.2017.08.030.
[20] R. Raso, L. Garcia, J. Ruiz, M. Oliva, J. Arauzo, Aqueous phase hydrogenolysis of glycerol over Ni/Al-Fe catalysts without external hydrogen addition, Appl. Catal. B Environ. 283 (2021), https://doi.org/10.1016/j.apcatb.2020.119598.
[21] B. Morales, B. Quesada, Conversion of glycerol to hydroxyacetone over Cu and Ni catalysts, Catal. Today 372 (2021) 115–125, https://doi.org/10.1016/j.cattod.2020.11.025.

[22] M. Velasquez, A. Santamaria, C. Batiot-Dupeyrat, Selective conversion of glycerol to hydroxyacetone in gas phase over La_2CuO_4 catalyst, Appl. Catal. B Environ. 160 (2014) 606–613, https://doi.org/10.1016/j.apcatb.2014.06.006.

[23] A. Talebian-Kiakalaieh, N. Amin, H. Hezaveh, Glycerol for renewable acrolein production by catalytic dehydration, Renew. Sustain. Energy Rev. 40 (2014) 28–59, https://doi.org/10.1016/j.rser.2014.07.168.

[24] F. Yang, M. Hanna, R. Sun, Value-added uses for crude glycerol-a byproduct of biodiesel production, Biotechnol. Biofuels 5 (2012), https://doi.org/10.1186/1754-6834-5-13.

[25] M. Nimlos, S. Blanksby, X. Qian, M. Himmel, D. Johnson, Mechanisms of glycerol dehydration, J. Phys. Chem. A 110 (18) (2006) 6145–6156, https://doi.org/10.1021/jp060597q.

[26] B. Katryniok, S. Paul, V. Bellière-Baca, P. Rey, F. Dumeignil, Glycerol dehydration to acrolein in the context of new uses of glycerol, Green Chem. 12 (12) (2010) 2079–2098, https://doi.org/10.1039/c0gc00307g.

[27] Y. Kim, K. Jung, E. Park, Gas-phase dehydration of glycerol over silica-alumina catalysts, Appl. Catal. B Environ. 107 (1–2) (2011) 177–187, https://doi.org/10.1016/j.apcatb.2011.07.011.

[28] S. Basu, V. Shree, A. Sen, Role of cerium as a promoter and process optimization studies for dehydration of glycerol to acetol over copper chromite catalyst, J. Rare Earths 40 (1) (2022) 63–72, https://doi.org/10.1016/j.jre.2021.01.013.

[29] A. Ulgen, W. Hoelderich, Conversion of glycerol to acrolein in the presence of WO_3/ZrO_2 catalysts, Catal. Lett. 131 (1–2) (2009) 122–128, https://doi.org/10.1007/s10562-009-9923-0.

[30] L. Ning, Y. Ding, W. Chen, L. Gong, R. Lin, Y. Lue, Q. Xin, Glycerol dehydration to acrolein over activated carbon-supported silicotungstic acids, Chin. J. Catal. 29 (3) (2008) 212–214, https://doi.org/10.1016/S1872-2067(08)60026-1.

[31] N. Shiju, D. Brown, K. Wilson, G. Rothenberg, Glycerol valorization: dehydration to acrolein over silica-supported niobia catalysts, Top. Catal. 53 (15–18) (2010) 1217–1223, https://doi.org/10.1007/s11244-010-9566-9.

[32] Y. Kim, K. Jung, E. Park, Gas-phase dehydration of glycerol over ZSM-5 catalysts, Microporous Mesoporous Mater. 131 (1–3) (2010) 28–36, https://doi.org/10.1016/j.micromeso.2009.11.037.

[33] H. Decolatti, B. Dalla Costa, C. Querini, Dehydration of glycerol to acrolein using H-ZSM5 zeolite modified by alkali treatment with NaOH, Microporous Mesoporous Mater. 204 (2015) 180–189, https://doi.org/10.1016/j.micromeso.2014.11.014.

[34] A. Alhanash, E. Kozhevnikova, I. Kozhevnikov, Gas-phase dehydration of glycerol to acrolein catalysed by caesium heteropoly salt, Appl. Catal. Gen. 378 (1) (2010) 11–18, https://doi.org/10.1016/j.apcata.2010.01.043.

[35] W. Suprun, M. Lutecki, T. Haber, H. Papp, Acidic catalysts for the dehydration of glycerol: activity and deactivation, J. Mol. Catal. Chem. 309 (1–2) (2009) 71–78, https://doi.org/10.1016/j.molcata.2009.04.017.

[36] A. Bienholz, H. Hofmann, P. Claus, Selective hydrogenolysis of glycerol over copper catalysts both in liquid and vapour phase: correlation between the copper surface area and the catalyst's activity, Appl. Catal. Gen. 391 (1–2) (2011) 153–157, https://doi.org/10.1016/j.apcata.2010.08.047.

[37] S. Sato, M. Akiyama, R. Takahashi, T. Hara, K. Inui, M. Yokota, Vapor-phase reaction of polyols over copper catalysts, Appl. Catal. Gen. 347 (2) (2008) 186–191, https://doi.org/10.1016/j.apcata.2008.06.013.

[38] C. Lago, H. Decolatti, L. Tonutti, B. Dalla Costa, C. Querini, Gas phase glycerol dehydration over H-ZSM-5 zeolite modified by alkaline treatment with Na_2CO_3, J. Catal. 366 (2018) 16–27, https://doi.org/10.1016/j.jcat.2018.07.036.

[39] C. Yue, M. Gan, L. Gu, Y. Zhuang, *In situ* synthesized nano-copper over ZSM-5 for the catalytic dehydration of glycerol under mild conditions, J. Taiwan Inst. Chem. Eng. 45 (4) (2014) 1443–1448, https://doi.org/10.1016/j.jtice.2014.01.005.

[40] T. Gabrysch, M. Muhler, B. Peng, The kinetics of glycerol hydrodeoxygenation to 1,2-propanediol over Cu/ZrO_2 in the aqueous phase, Appl. Catal. Gen. 576 (2019) 47–53, https://doi.org/10.1016/j.apcata.2019.03.001.

[41] Q. Liu, X. Cao, T. Wang, C. Wang, Q. Zhang, L. Ma, Synthesis of shape-controllable cobalt nanoparticles and their shape-dependent performance in glycerol hydrogenolysis, RSC Adv. 5 (7) (2015) 4861–4871, https://doi.org/10.1039/c4ra13395a.

[42] C. Chiu, M. Dasari, G. Suppes, W. Sutterlin, Dehydration of glycerol to acetol via catalytic reactive distillation, AIChE J. 52 (10) (2006) 3543–3548, https://doi.org/10.1002/aic.10951.

[43] S. Basu, A. Sen, M. Mukherjee, Synthesis and performance evaluation of silica-supported copper chromite catalyst for glycerol dehydration to acetol, J. Chem. Sci. 131 (8) (2019), https://doi.org/10.1007/s12039-019-1662-1.

[44] N. Pandhare, S. Pudi, P. Biswas, S. Sinha, Vapor phase hydrogenolysis of glycerol to 1,2-propanediol over gamma-Al_2O_3 supported copper or nickel monometallic and copper-nickel bimetallic catalysts, J. Taiwan Inst. Chem. Eng. 61 (2016) 90–96, https://doi.org/10.1016/j.jtice.2015.12.028.

[45] A. Seretis, P. Tsiakaras, Hydrogenolysis of glycerol to propylene glycol by in situ produced hydrogen from aqueous phase reforming of glycerol over SiO_2-Al_2O_3 supported nickel catalyst, Fuel Process. Technol. 142 (2016) 135–146, https://doi.org/10.1016/j.fuproc.2015.10.013.

[46] M. Dasari, P. Kiatsimkul, W. Sutterlin, G. Suppes, Low-pressure hydrogenolysis of glycerol to propylene glycol, Appl. Catal. Gen. 281 (1–2) (2005) 225–231, https://doi.org/10.1016/j.apcata.2004.11.033.

[47] C. Montassier, D. Giraud, J. Barbier, J. Boitiaux, Polyol transformation by liquid-phase heterogeneous catalysis over metals, Bull. Soc. Chim. Fr. (2) (1989) 148–155.

[48] B. Miranda, R. Chimentao, J. Szanyi, A. Braga, J. Santos, F. Gispert-Guirado, J. Llorca, F. Medina, Influence of copper on nickel-based catalysts in the conversion of glycerol, Appl. Catal. B Environ. 166 (2015) 166–180, https://doi.org/10.1016/j.apcatb.2014.11.019.

[49] A. Lete, R. Raso, L. Garcia, J. Ruiz, J. Arauzo, Synthesis of ketones from glycerol and 1,2-propanediol using copper and nickel catalysts: unraveling the impact of reaction phase and active metal, Fuel 371 (2024) 132001, https://doi.org/10.1016/j.fuel.2024.132001.

[50] A. Lete, F. Lacleta, L. García, J. Ruiz, J. Arauzo, Effect of calcination temperature and atmosphere on the properties and performance of CuAl catalysts for glycerol dehydration to acetol, Biomass Bioenergy 195 (2025), https://doi.org/10.1016/j.biombioe.2025.107725.

[51] M. García, L. Botella, N. Gil-Lalaguna, J. Arauzo, A. Gonzalo, J. Sánchez, Antioxidants for biodiesel: additives prepared from extracted fractions of bio-oil, Fuel Process. Technol. 156 (2017) 407–414, https://doi.org/10.1016/j.fuproc.2016.10.001.

[52] R. Raso, E. Abad, L. García, J. Ruíz, M. Oliva, J. Arauzo, Renewable hydrogen production by aqueous phase reforming of pure/refined crude glycerol over Ni/Al-Ca catalysts, Molecules 28 (18) (2023) 6695, https://doi.org/10.3390/molecules28186695.

[53] J. Remón, J. Giménez, A. Valiente, L. García, J. Arauzo, Production of gaseous and liquid chemicals by aqueous phase reforming of crude glycerol: influence of operating conditions on the process, Energy Convers. Manag. 110 (2016) 90–112, https://doi.org/10.1016/j.enconman.2015.11.070.

[54] J. Fermoso, L. He, D. Chen, Production of high purity hydrogen by sorption enhanced steam reforming of crude glycerol, Int. J. Hydrogen Energy 37 (19) (2012) 14047–14054, https://doi.org/10.1016/j.ijhydene.2012.07.084.

[55] M. Thommes, K. Kaneko, A. Neimark, J. Olivier, F. Rodriguez-Reinoso, J. Rouquerol, K. Sing, Physisorption of gases, with special reference to the evaluation of surface area and pore size distribution (IUPAC Technical Report), Pure Appl. Chem. 87 (9–10) (2015) 1051–1069, https://doi.org/10.1515/pac-2014-1117.

[56] R. Mane, A. Yamaguchi, A. Malawadkar, M. Shirai, C. Rode, Active sites in modified copper catalysts for selective liquid phase dehydration of aqueous glycerol to acetol, RSC Adv. 3 (37) (2013) 16499–16508, https://doi.org/10.1039/c3ra42348d.

[57] T. Braga, N. Essayem, S. Prakash, A. Valentini, Gas-phase conversion of glycerol to acetol: influence of support acidity on the catalytic stability and copper surface properties on the activity, J. Braz. Chem. Soc. 27 (12) (2016) 2361–2371, https://doi.org/10.5935/0103-5053.20160134.

[58] M. Luo, P. Fang, M. He, Y. Xie, In situ XRD, Raman, and TPR studies of CuO/Al_2O_3 catalysts for CO oxidation, J. Mol. Catal. Chem. 239 (1–2) (2005) 243–248, https://doi.org/10.1016/j.molcata.2005.06.029.

[59] G. Foo, D. Wei, D. Sholl, C. Sievers, Role of Lewis and bronsted acid sites in the dehydration of glycerol over niobia, ACS Catal. 4 (9) (2014) 3180–3192, https://doi.org/10.1021/cs5006376.

[60] J. Lif, I. Odenbrand, M. Skoglundh, Sintering of alumina-supported nickel particles under amination conditions: support effects, Appl. Catal. Gen. 317 (1) (2007) 62–69, https://doi.org/10.1016/j.apcata.2006.10.003.

[61] R. Mane, C. Rode, Simultaneous glycerol dehydration and in situ hydrogenolysis over Cu-Al oxide under an inert atmosphere, Green Chem. 14 (10) (2012) 2780–2789, https://doi.org/10.1039/c2gc35661a.

[62] M. Behrens, Coprecipitation: an excellent tool for the synthesis of supported metal catalysts - from the understanding of the well known recipes to new materials, Catal. Today 246 (2015) 46–54, https://doi.org/10.1016/j.cattod.2014.07.050.

[63] C. Tang, J. Sun, X. Yao, Y. Cao, L. Liu, C. Ge, F. Gao, L. Dong, Efficient fabrication of active CuO-CeO_2/SBA-15 catalysts for preferential oxidation of CO by solid state impregnation, Appl. Catal. B Environ. 146 (2014) 201–212, https://doi.org/10.1016/j.apcatb.2013.05.060.

[64] J. Mazarío, P. Concepción, M. Ventura, M. Domine, Continuous catalytic process for the selective dehydration of glycerol over Cu-based mixed oxide, J. Catal. 385 (2020) 160–175, https://doi.org/10.1016/j.jcat.2020.03.010.

[65] M. D'Angelo, V. Ordomsky, J. van der Schaaf, J. Schouten, T. Nijhuis, Continuous hydrogen stripping during aqueous phase reforming of sorbitol in a washcoated microchannel reactor with a Pt-Ru bimetallic catalyst, Int. J. Hydrogen Energy 39 (31) (2014) 18069–18076, https://doi.org/10.1016/j.ijhydene.2014.02.167.

[66] B. Dou, G. Rickett, V. Dupont, P. Williams, H. Chen, Y. Ding, M. Ghadiri, Steam reforming of crude glycerol with in situ CO_2 sorption, Bioresour. Technol. 101 (7) (2010) 2436–2442, https://doi.org/10.1016/j.biortech.2009.10.092.

[67] T. Valliyappan, D. Ferdous, N. Bakhshi, A. Dalai, Production of hydrogen and syngas via steam gasification of glycerol in a fixed-bed reactor, Top. Catal. 49 (1–2) (2008) 59–67, https://doi.org/10.1007/s11244-008-9062-7.

[68] J. Remon, V. Mercado, L. Garcia, J. Arauzo, Effect of acetic acid, methanol and potassium hydroxide on the catalytic steam reforming of glycerol: thermodynamic and experimental study, Fuel Process. Technol. 138 (2015) 325–336, https://doi.org/10.1016/j.fuproc.2015.05.034.

[69] H. Atia, U. Armbruster, A. Martin, Dehydration of glycerol in gas phase using heteropolyacid catalysts as active compounds, J. Catal. 258 (1) (2008) 71–82, https://doi.org/10.1016/j.jcat.2008.05.027.

[70] E. Vasiliadou, A. Lemonidou, Investigating the performance and deactivation behaviour of silica-supported copper catalysts in glycerol hydrogenolysis, Appl. Catal. Gen. 396 (1–2) (2011) 177–185, https://doi.org/10.1016/j.apcata.2011.02.014.

[71] M. Twigg, M. Spencer, Deactivation of supported copper metal catalysts for hydrogenation reactions, Appl. Catal. Gen. 212 (1–2) (2001) 161–174, https://doi.org/10.1016/S0926-860X(00)00854-1.

[72] M. Twigg, M. Spencer, Deactivation of copper metal catalysts for methanol decomposition, methanol steam reforming and methanol synthesis, Top. Catal. 22 (3–4) (2003) 191–203, https://doi.org/10.1023/A:1023567718303.

[73] A. Konaka, T. Tago, T. Yoshikawa, H. Shitara, Y. Nakasaka, T. Masuda, Conversion of biodiesel-derived crude glycerol into useful chemicals over a zirconia-iron oxide catalyst, Ind. Eng. Chem. Res. 52 (44) (2013) 15509–15515, https://doi.org/10.1021/ie4006645.
[74] T. Rajkhowa, G. Marin, J. Thybaut, Quantifying the dominant factors in Cu catalyst deactivation during glycerol hydrogenolysis, J. Ind. Eng. Chem. 54 (2017) 270–277, https://doi.org/10.1016/j.jiec.2017.05.040.
[75] B. Sereshki, S. Balan, G. Patience, J. Dubois, Reactive vaporization of crude glycerol in a fluidized bed reactor, Ind. Eng. Chem. Res. 49 (3) (2010) 1050–1056, https://doi.org/10.1021/ie9006968.
[76] F. Maldonado-Martín, L. García, J. Ruiz, M. Oliva, J. Arauzo, Selective conversion of glycerol to acetol: effect of the preparation method of CuAl catalysts and reaction phase, Catalysts 15 (4) (2025), https://doi.org/10.3390/catal15040348.
[77] J. Jang, S. Zhu, E. Delmo, T. Li, Q. Zhao, Y. Wang, L. Zhang, H. Huang, J. Ge, M. Shao, Facile design of oxide-derived Cu nanosheet electrocatalyst for CO_2 reduction reaction, Ecomat 5 (5) (2023), https://doi.org/10.1002/eom2.12334.
[78] H. Park, Y. Yun, T. Kim, K. Lee, J. Baek, J. Yi, Kinetics of the dehydration of glycerol over acid catalysts with an investigation of deactivation mechanism by coke, Appl. Catal. B Environ. 176 (2015) 1–10, https://doi.org/10.1016/j.apcatb.2015.03.046.
[79] J. Barrault, J. Clacens, Y. Pouilloux, Selective oligomerization of glycerol over mesoporous catalysts, Top. Catal. 27 (1–4) (2004) 137–142, https://doi.org/10.1023/B:TOCA.0000013548.16699.1c.
[80] J. Clacens, Y. Pouilloux, J. Barrault, Selective etherification of glycerol to polyglycerols over impregnated basic MCM-41 type mesoporous catalysts, Appl. Catal. Gen. 227 (1–2) (2002) 181–190, https://doi.org/10.1016/S0926-860X(01)00920-6.
[81] N. Charisiou, S. Douvartzides, G. Siakavelas, L. Tzounis, V. Sebastian, V. Stolojan, S. Hinder, M. Baker, K. Polychronopoulou, M. Goula, The relationship between reaction temperature and carbon deposition on nickel catalysts based on Al_2O_3, ZrO_2 or SiO_2 supports during the biogas dry reforming reaction, Catalysts 9 (8) (2019), https://doi.org/10.3390/catal9080676.
[82] M. Velasquez, C. Batiot-Dupeyrat, J. Gallego, J. Fernández, A. Santamaria, Synthesis of carbon nano-chains from glycerol-ethanol decomposition over Ni-Fe alloy catalyst, Diam. Relat. Mater. 70 (2016) 105–113, https://doi.org/10.1016/j.diamond.2016.10.019.
[83] G. Catuzo, L. Possato, M. Sad, C. Padró, L. Martins, Progress of the catalytic deactivation of H-ZSM-5 zeolite in glycerol dehydration, ChemCatChem 13 (20) (2021) 4419–4430, https://doi.org/10.1002/cctc.202100576.
[84] P. Lauriol-Garbay, J. Millet, S. Loridant, V. Bellière-Baca, P. Rey, New efficient and long-life catalyst for gas-phase glycerol dehydration to acrolein, J. Catal. 280 (1) (2011) 68–76, https://doi.org/10.1016/j.jcat.2011.03.005.
[85] W. Cheng, Deactivation and regeneration of Cu/Cr based methanol decomposition catalysts, Appl. Catal. B Environ. 7 (1–2) (1995) 127–136, https://doi.org/10.1016/0926-3373(95)00187-5.
[86] A. Reinsdorf, W. Korth, A. Jess, M. Terock, F. Klasovsky, R. Franke, Insights into deactivation and regeneration of an industrial Cu/Ni/Cr-Al_2O_3 catalyst during aldehyde hydrogenation, ChemCatChem 8 (23) (2016) 3592–3599, https://doi.org/10.1002/cctc.201601022.